Article

Developmental Cell

Concerted Action of Evolutionarily Ancient and Novel SNARE Complexes in Flowering-Plant Cytokinesis

Highlights

- Qa-SNAREs SYP132 and KNOLLE function in cytokinesis in *Arabidopsis*
- SYP132 also functions in the secretory pathway, unlike KNOLLE
- KNOLLE is an evolutionarily derived Qa-SNARE specializing in angiosperm cytokinesis
- SYP132 is a non-specialized ancient Qa-SNARE originating in alga-like ancestors

Authors

Misoon Park, Cornelia Krause, Matthias Karnahl, ..., Jeffery L. Dangl, Anton A. Sanderfoot, Gerd Jürgens

Correspondence

gerd.juergens@zmbp.uni-tuebingen.de

In Brief

In plant cytokinesis, SNARE complexes mediate vesicle fusion for partitioning membrane formation. Park et al. show that evolutionarily ancient Qa-SNARE SYP132 functionally overlaps with flowering plant- and cytokinesis-specific Qa-SNARE KNOLLE. KNOLLE acquisition may have been due to high demand for membrane-fusion capacity during endosperm cellularization in flowering plants.

Park et al., 2018, Developmental Cell *44*, 1–12
February 26, 2018
https://doi.org/10.1016/j.devcel.2017.12.027

CellPress

Please cite this article in press as: Park et al., Concerted Action of Evolutionarily Ancient and Novel SNARE Complexes in Flowering-Plant Cytokinesis, Developmental Cell (2017), https://doi.org/10.1016/j.devcel.2017.12.027

Developmental Cell
Article

Concerted Action of Evolutionarily Ancient and Novel SNARE Complexes in Flowering-Plant Cytokinesis

Misoon Park,[1] Cornelia Krause,[1,7] Matthias Karnahl,[1] Ilka Reichardt,[1,8] Farid El Kasmi,[1,9] Ulrike Mayer,[1,2] York-Dieter Stierhof,[2] Ulrike Hiller,[1,2] Georg Strompen,[1,10] Martin Bayer,[3] Marika Kientz,[1] Masa H. Sato,[4] Marc T. Nishimura,[5,11] Jeffery L. Dangl,[5] Anton A. Sanderfoot,[6] and Gerd Jürgens[1,12,*]

[1]Center for Plant Molecular Biology (ZMBP), Developmental Genetics, University of Tübingen, Auf der Morgenstelle 32, 72076 Tübingen, Germany
[2]Center for Plant Molecular Biology (ZMBP), Microscopy, University of Tübingen, 72076 Tübingen, Germany
[3]Department of Cell Biology, Max Planck Institute for Developmental Biology, 72076 Tübingen, Germany
[4]Laboratory of Cellular Dynamics, Graduate School of Life and Environmental Sciences, Kyoto Prefectural University, Kyoto 606-8522, Japan
[5]Department of Biology, University of North Carolina, Chapel Hill, NC 27599, USA
[6]Biology Department, University of Wisconsin La Crosse, La Crosse, WI 54601, USA
[7]Present address: Staatliches Museum für Naturkunde Stuttgart, 70191 Stuttgart, Germany
[8]Present address: Gregor Mendel Institute, 1030 Vienna, Austria
[9]Present address: Department of Biology, University of North Carolina, Chapel Hill, NC 27599, USA
[10]Present address: UP-Transfer GmbH, Universität Potsdam, 14669 Potsdam, Germany
[11]Present address: Department of Biochemistry & Molecular Biology, Colorado State University, Fort Collins, CO 80523, USA
[12]Lead Contact
*Correspondence: gerd.juergens@zmbp.uni-tuebingen.de
https://doi.org/10.1016/j.devcel.2017.12.027

SUMMARY

Membrane vesicles delivered to the cell-division plane fuse with one another to form the partitioning membrane during plant cytokinesis, starting in the cell center. In *Arabidopsis*, this requires SNARE complexes involving the cytokinesis-specific Qa-SNARE KNOLLE. However, cytokinesis still occurs in *knolle* mutant embryos, suggesting contributions from KNOLLE-independent SNARE complexes. Here we show that Qa-SNARE SYP132, having counterparts in lower plants, functionally overlaps with the flowering plant-specific KNOLLE. *SYP132* mutation causes cytokinesis defects, *knolle syp132* double mutants consist of only one or a few multi-nucleate cells, and SYP132 has the same SNARE partners as KNOLLE. SYP132 and KNOLLE also have non-overlapping functions in secretion and in cellularization of the embryo-nourishing endosperm resulting from double fertilization unique to flowering plants. Evolutionarily ancient non-specialized SNARE complexes originating in algae were thus amended by the appearance of cytokinesis-specific SNARE complexes, meeting the high demand for membrane-fusion capacity during endosperm cellularization in angiosperms.

INTRODUCTION

Plants and non-plant eukaryotes diverged in evolution from single cells more than one billion years ago (Hedges et al., 2004; Yoon et al., 2004). Both fungal and animal cells initiate cytokinesis at the plasma membrane, with the formation of a contractile actomyosin ring that constricts the cell from the periphery, resulting in a central cytoplasmic bridge ("midbody") between the forming daughter cells, which is eventually severed by ESCRTIII-mediated constriction ("abscission") (Mierzwa and Gerlich, 2014). There are SNARE proteins localizing to the midbody (Low et al., 2003; Gromley et al., 2005). However, their role in abscission is controversial (Nakayama, 2016). Although contributing to furrow extension, membrane traffic appears to play a rather indirect role in animal cytokinesis (Schiel and Prekeris, 2013). In contrast, plant cells initiate cytokinesis in the center of the division plane through the targeted delivery of *trans*-Golgi network-derived secretory membrane vesicles, which fuse with one another to form the partitioning membrane known as the cell plate (Richter et al., 2014). This plant-specific mode of cytokinesis requires the assistance of a dynamic cytoskeletal array called the phragmoplast whose center-out remodeling drives centrifugal expansion of the cell plate until the margin of the latter fuses with the parental plasma membrane (Staehelin and Hepler, 1996).

Membrane fusion requires the formation of SNARE complexes that bridge the gap between adjacent membranes. Mutant analysis in the flowering plant *Arabidopsis* identified two genes specifically required for membrane vesicle fusion in cytokinesis: *KNOLLE*, encoding a cytokinesis-specific Qa-SNARE, and *KEULE*, encoding a KNOLLE-interacting Sec1/Munc18 protein (Lukowitz et al., 1996; Lauber et al., 1997; Assaad et al., 2001; Park et al., 2012). KNOLLE forms two kinds of SNARE complexes that act redundantly in cytokinesis: a trimeric complex comprising KNOLLE and its partners Qbc-SNARE SNAP33 and R-SNARE VAMP721 or VAMP722, whereas the other, tetrameric complex comprises KNOLLE and its partners Qb-SNARE

NPSN11, Qc-SNARE SYP71, and also R-SNARE VAMP721 or VAMP722 (El Kasmi et al., 2013). Interestingly, loss of *KNOLLE* function does not arrest embryo development at the zygote stage, indicating that cytokinesis is not completely blocked. In contrast, the *knolle keule* double-mutant embryo dies as a huge single cell with many nuclei, with no trace of cytokinesis detectable (Waizenegger et al., 2000). Thus, the membrane-fusion machinery appears to be more complex, with other Qa-SNAREs also forming SNARE complexes that contribute to cytokinesis. KNOLLE (also known as SYP111) is a member of the SYP1 family of "plasma membrane" Qa-SNAREs (Enami et al., 2009). Its closest relative, SYP112, essentially behaves like KNOLLE if expressed like KNOLLE. However, *SYP112* is not essential, and the *knolle syp112* double mutant looks identical to the *knolle* single mutant (Müller et al., 2003).

The plant-specific mode of phragmoplast-assisted cytokinesis originated within the clade of green algae that gave rise to land plants (Sawitzky and Grolig, 1995; Cook, 2004; Buschmann and Zachgo, 2016). In contrast, cytokinesis-specific Qa-SNARE KNOLLE appears to have arisen only with the advent of angiosperms several hundred million years later (Sanderfoot, 2007; see below). A possible candidate Qa-SNARE contributing to cytokinesis is the plasma membrane-localized SYP132, which is evolutionarily conserved in the plant lineage and able to complement *Arabidopsis knolle* mutant plants when expressed from the *KNOLLE* promoter (Sanderfoot, 2007; Reichardt et al., 2011). SYP132 appears to play diverse biological roles in different plant species. It is involved in biotic interactions, such as pathogen defense in tobacco and wheat, and nitrogen-fixing symbiosome formation and arbuscular mycorrhiza interactions in *Medicago* (Catalano et al., 2007; Kalde et al., 2007; Limpens et al., 2009; Pan et al., 2016; Wang et al., 2014; Huisman et al., 2016). In *Arabidopsis*, SYP132 mediates tip growth of root hairs, as indicated by conditional root hair defects caused by inducible knock down (Ichikawa et al., 2014). Importantly, *Arabidopsis* SYP132 protein does not cycle between the plasma membrane and endosomes in interphase, and is thus not retargeted in cytokinesis. Rather it accumulates as a newly synthesized protein in the cell-division plane (Enami et al., 2009; Reichardt et al., 2011). SYP132 forms an SDS-resistant SNARE complex with Qbc-SNARE SNAP33 and R-SNARE VAMP721 or VAMP722 *in vitro* when the proteins are mixed in equimolar amounts (Yun et al., 2013). SYP132 also interacts with VAMP721, VAMP722, and VAMP724, but not VAMP723, in split-luciferase complementation assays in transfected protoplasts (Ichikawa et al., 2014). In addition, Qb-SNAREs NPSN11 and NPSN13, and Qc-SNARE SYP71 and R-SNARE VAMP721, have been identified as SYP132 interactors by mass spectrometric analysis of immunoprecipitate from transgenic *Arabidopsis* plants (Fujiwara et al., 2014).

Here we address two puzzling questions regarding the membrane-fusion machinery in *Arabidopsis* cytokinesis and its evolutionary origin: (1) Why does the knock out of the cytokinesis-specific Qa-SNARE KNOLLE not prevent cytokinesis at the zygote stage of embryogenesis? (2) Might this residual capacity for cytokinesis provide clues to the evolution of present-day angiosperm cytokinesis, compared with the phragmoplast-assisted cytokinesis that occurs in the absence of the cytokinesis-specific Qa-SNARE KNOLLE in lower plants? Our results suggest that the Qa-SNARE SYP132, a member of an ancient clade present already in charophyte algae, interacts with the SNARE partners of KNOLLE to form evolutionarily ancient but still active SNARE complexes, which serve both secretory and cytokinetic membrane fusion in *Arabidopsis*. This contrasts with KNOLLE, which only arose with the advent of flowering plants, and specifically mediates formation of the partitioning membrane in cytokinesis and endosperm cellularization.

RESULTS

Zygotic Disruption of *SYP132* Gene Function Results in *Knolle*-like Cytokinesis-Defective Embryo and Seedling Phenotypes

The Qa-SNARE KNOLLE is the only one of nine *Arabidopsis* members of the SYP1 family of plasma membrane Qa-SNAREs that is strongly expressed during late-G2 to M phase, and turned over rapidly at the end of cytokinesis (Lukowitz et al., 1996; Lauber et al., 1997; Müller et al., 2003; Reichardt et al., 2007, 2011; Sanderfoot, 2007). Unlike KNOLLE, SYP132 is uniformly expressed in all organs and at all stages, stably accumulating at the plasma membrane (Enami et al., 2009; Schmid et al., 2005). However, SYP132 also accumulates at the plane of cell division, which appears to depend on *de novo* synthesis during late-G2 to M phase (Enami et al., 2009; Reichardt et al., 2011). Furthermore, SYP132 is functionally similar to KNOLLE in that it can rescue *knolle* mutant plants when expressed from the *KNOLLE* promoter, whereas another SYP1 family Qa-SNARE PEN1 (also known as SYP121) involved in pathogen defense and K+ channel regulation is unable to do so (Collins et al., 2003; Grefen et al., 2010; Reichardt et al., 2011). Unfortunately, there is no *syp132* knockout mutant available. Attempts to identify ethyl methanesulfonate-induced knockouts by TILLING were also unsuccessful, yielding only functionally intact variants (Figure S1A; mutations R210H and D230N when introduced into KNOLLE as R218H and D238N did not compromise KNOLLE function, as indicated by the ability of these KNOLLE variants to rescue *knolle* mutant plants) (Till et al., 2003). A transfer DNA (T-DNA) insertion in the promoter region of *SYP132* (*syp132*^{T}) showed a comparatively weak phenotype: bushy plants with almost no seeds, and the seedlings also seemed to be abnormal because they often formed adventitious roots instead of a single primary root (Figures 1B and S1B–E). The *syp132*^{T} mutant embryos displayed a mild phenotype and were often indistinguishable from wild-type embryos (Figures 1G and S2A–S2D). This *syp132*^{T} mutant was restored by the expression of transgene *SYP132::GFP-SYP132* (Figure S1K), indicating the specificity of *syp132*^{T}. To obtain an independent mutant allele of *SYP132*, we generated an artificial microRNA construct, using the Artificial microRNA Designer program (Schwab et al., 2006). Two-component expression of *amiR(SYP132)* from a strong ribosomal protein promoter, which is active in embryogenesis from fertilization onward (Weijers et al., 2003), (*RPS5A::GAL4* X *UAS::amiR*(*SYP132*), abbreviated as *syp132*^{amiR}), caused abnormal seedlings. These seedlings displayed a disorganized shoot meristem and the hallmarks of defective cytokinesis, such as multi-nucleate cells, cell-wall stubs, cell-wall fragments, and a band of unfused vesicles in the plane of cell division

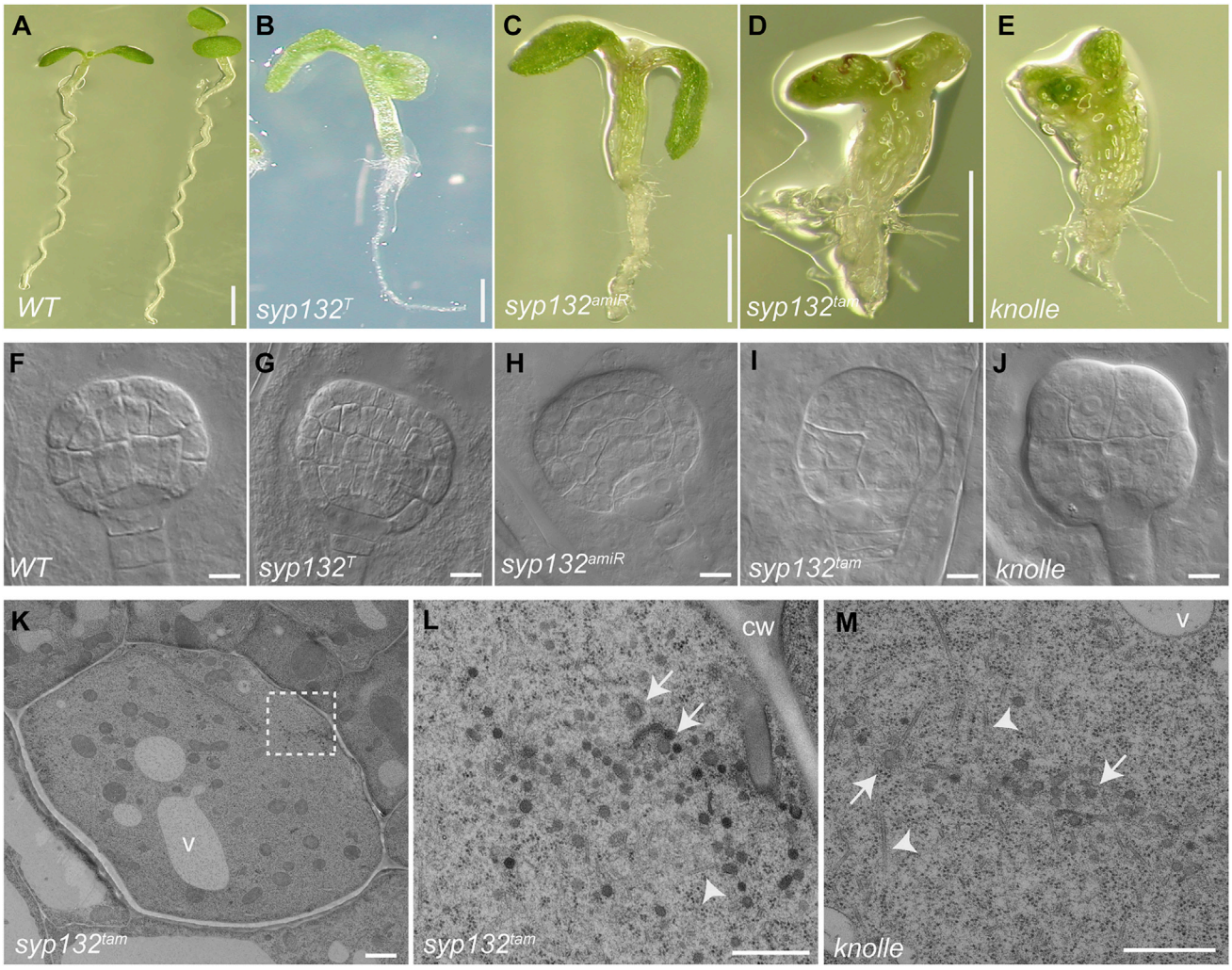

Figure 1. *syp132* Mutants Displaying Defects in Cytokinesis

(A–J) Seedlings (A–E), embryos (F–J): wild-type (A and F), *syp132*^{T} (B and G), *syp132*^{amiR} (C and H), *syp132*^{tam} (D and I), and *knolle* (E and J).

(K–M) Transmission electron microscopy (TEM) image after cryo-fixation and freeze-substitution of *syp132*^{tam} (K and L), (L) boxed area in (K) at higher magnification, and *knolle* (M); note unfused vesicles (arrows) near microtubule arrays (arrowheads) in the plane of cell division (L and M).

For genetic analysis, see Tables S1 and S2. WT, wild-type. Scale bars, 5 mm (A and B); 1 mm (C–E); 10 μm (F–J); 1 μm (K); and 0.5 μm (L and M). See also Figures S1 and S2 and Tables S1, S2, and S4.

(Figures 1C and S1F–S1J). Thus, Qa-SNARE SYP132 is required for cytokinesis. Like the *syp132*^{T} allele, the *syp132*^{amiR} mutant presented a relatively mild phenotype in developing embryos (Figures 1H and S2E–S2H). To verify that the mutant phenotype was caused by the artificial microRNA against *SYP132*, we generated a *SYP132_SYP123* chimeric gene that was resistant to *amiR(SYP132)* because the relevant sequence was no longer complementary to the artificial microRNA. *SYP123* is a close homolog of *SYP132*, and encodes the same peptide sequence from the different *amiR(SYP132)* target sequence. As expected, *KNOLLE::vYFP:SYP132_SYP123* rescued the *syp132*^{amiR} mutant (Figures S1L–S1N), revealing that *SYP132* is the specific target of *amiR*(*SYP132*). Then we combined *syp132*^{amiR} with the *syp132*^{T} allele for generating a *SYP132* mutant with an enhanced mutant phenotype, which we named two-alleles mutant of *syp132* (*syp132*^{tam}). The *syp132*^{tam} mutant embryos and seedlings displayed mutant phenotypes that were nearly indistinguishable from *knolle* mutant embryos and seedlings, respectively (Figures 1D and 1I, compare with 1E and 1J; Figures S2I–S2L). Notably, the *syp132*^{tam} embryos had cytokinesis defects including variably enlarged multi-nucleate cells, sometimes with enlarged nuclei. Like *knolle* mutant embryos, these *syp132*^{tam} embryos displayed bands of unfused vesicles (Figures 1K and 1L, compare with 1M). These results suggested that SYP132 plays an important role in cytokinesis. Since SYP132 protein accumulates at the plasma membrane in interphase (Enami et al., 2009; Reichardt et al., 2011), we also examined effects on secretory trafficking in *syp132*^{tam} mutant embryos/seedlings, using the cell-wall hemicellulosic polysaccharide xyloglucan (detectable with monoclonal antibody CCRC-M1) as a marker for secretion from the cell (Stierhof and El Kasmi, 2010; Zhang and Staehelin, 1992). Unlike wild-type

Please cite this article in press as: Park et al., Concerted Action of Evolutionarily Ancient and Novel SNARE Complexes in Flowering-Plant Cytokinesis, Developmental Cell (2017), https://doi.org/10.1016/j.devcel.2017.12.027

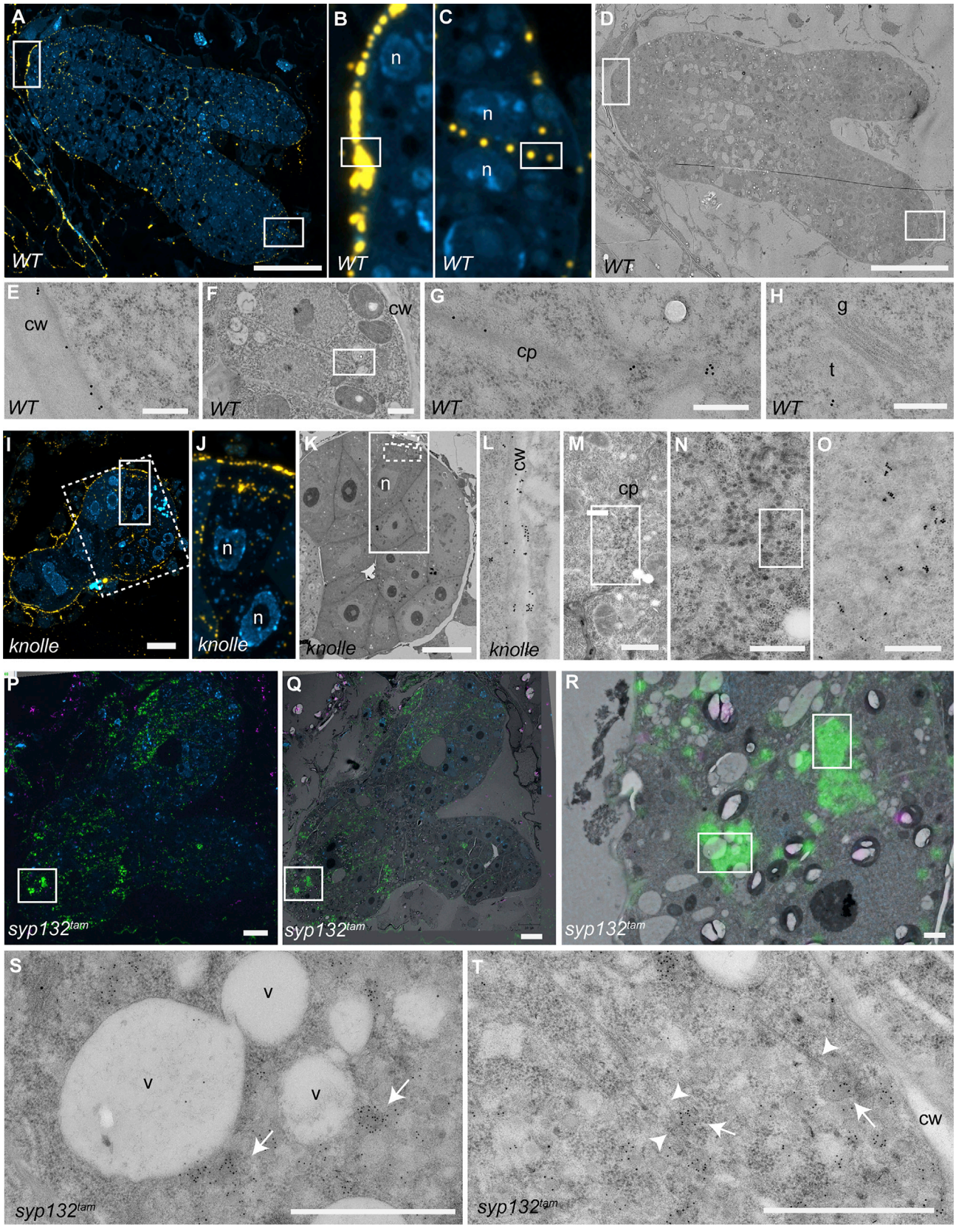

(legend on next page)

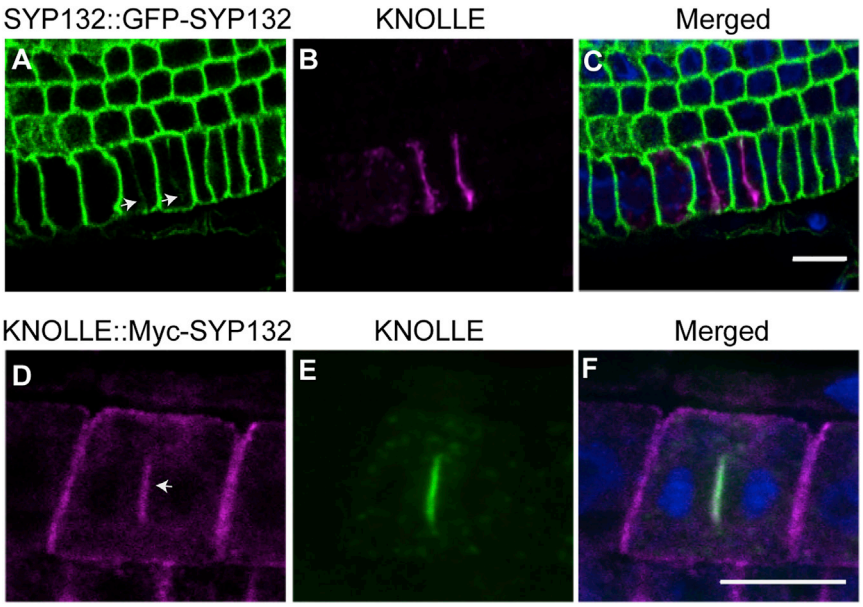

Figure 3. Subcellular Localization of Qa-SNAREs SYP132 and KNOLLE in Seedling Root Cells

(A–C) Co-localization of (A) SYP132::GFP-SYP132 (green), and (B) KNOLLE (magenta) labeled with anti-KNOLLE antiserum; (C) merged image plus DAPI staining of chromatin (blue).

(D–F) Co-localization of (D) KNOLLE::Myc-SYP132 (magenta) and (E) KNOLLE (green) labeled with anti-Myc and anti-KNOLLE antisera, respectively; (F) merged image plus DAPI staining of chromatin (blue).

Arrows indicate planes of cell division (A and D). Scale bars, 10 μm (C and F). See also Figures S3 and S4.

and *knolle* mutant embryos, which displayed an undisturbed extracellular accumulation of xyloglucan, *syp132^{tam}* mutant embryos accumulated massive amounts of the secretory marker in intracellular membrane vesicles (Figures 2A–2T). In conclusion, Qa-SNARE SYP132 appears to be required, like KNOLLE, for making the partitioning membrane in cytokinesis. Unlike KNOLLE, however, SYP132 appears to be also required for secretory trafficking to the plasma membrane in interphase.

Subcellular Localization of SYP132 Relative to KNOLLE in Cytokinesis

Unlike *KNOLLE*, *SYP132* mRNA is expressed at high level essentially in all cells of all developmental stages (Figure S3A) (Schmid et al., 2005). SYP132 protein fused to GFP and, expressed from the *SYP132* regulatory sequences, accumulated strongly at the plasma membrane but only weakly in the cell-division plane (Figures 3A–3C and S3B–S3D) (Enami et al., 2009). However, expression of SYP132 from the *KNOLLE* promoter yielded comparable accumulation of SYP132 to endogenous KNOLLE in the plane of cell division (Figures 3D–3F) and rescued the *knolle* deletion mutant (Reichardt et al., 2011). These different levels of expression correlate with the presence of two mitosis-specific activator (MSA) sequences that are close to each other in the *KNOLLE* promoter (Haga et al., 2007), but more than 100 base pairs apart in the *SYP132* promoter (Figure S4). The two closely spaced MSA elements in the *KNOLLE* promoter are essential for expression and KNOLLE function in cytokinesis (Haga et al., 2007). In contrast, *SYP132::GFP-SYP132* rescued the *knolle* mutant only partially, whereas it rescued the *syp132^{T}* mutant fully (Figure S1K; Table S3), suggesting that the MSA elements in the *SYP132* promoter are not sufficient for expressing the required amount of SYP132 protein in cytokinesis.

Nearly Complete Inhibition of Cytokinesis in *Knolle syp132^{tam}* Double Mutants

If both KNOLLE and SYP132 contributed to cytokinesis, then the *knolle syp132^{tam}* double mutant should exhibit a much stronger phenotype than either single mutant alone. Indeed, the double mutant was embryo lethal, whereas each single mutant completed embryogenesis, dying as abnormal seedlings (Figure 4; compare with Figures 1F–1J). *knolle syp132^{amiR}* or *knolle syp132^{T}* embryos consisted of a few multi-nucleate cells (Figures 4C and 4D; Table S1). Analysis of *knolle syp132^{tam}* yielded a high proportion of single-celled to few-celled embryos with multiple

Figure 2. *syp132* Mutants Displaying Defects in Secretory Pathway

Immunolocalization of xyloglucan in cryo-fixed and freeze-substituted embryos.

(A–H) Wild-type embryo (torpedo stage). (A–C) Fluorescently labeled xyloglucan (yellow): (B and C), enlarged boxes in (A) showing signals at cell wall (B) and in the plane of cell division (C). (D–H) Gold-labeled xyloglucan: (D) neighboring section (overview) imaged by TEM; (E) gold labeling of the cell wall in the region marked in (B) (white box); (F–G) gold labeling of cell plate shown in (C) (white box); (G) enlarged box in (F); (H) Golgi apparatus (G) with gold labeling in the *trans*-Golgi network (t). Note fluorescence and gold labeling on neighboring sections of the identical specimen block.

(I–O) *knolle* embryo (globular stage). (I and J) Fluorescently labeled xyloglucan; (J), enlarged detail of white box in (I). (K–O) Gold-labeled xyloglucan: (K) gold labeling of dashed box in (I); (L) enlarged view of smaller dashed box (K) showing cell wall labeling; (M) enlarged detail of bigger dashed box (K) showing cell plate labeling; (N) enlarged detail of (M) (white box) showing cell wall stubs and unfused vesicles between them; (O) same region of (M) showing vesicles. Note fluorescence and gold labeling on neighboring sections of the identical specimen block.

(P–T) *syp132^{tam}* embryo (torpedo stage). (P–R) Fluorescently labeled xyloglucan (green): (Q) overlay of fluorescence image and TEM image showing the identical section; (R) enlarged detail of (Q). Note that large numbers of fluorescent secretory vesicles are accumulated in intracellular region, unlike in wild-type and *knolle*. (S and T) Gold-labeled xyloglucan: (S) gold labeling of a region marked in (R); (T) gold labeling of the second region marked in (R) (rotated by 90°). Several microtubules, arrows in (T) are indicative of a cell plate with a large number of xyloglucan-positive unfused vesicles, arrowheads in (S) and (T). The light magenta color represents starch non-specifically labeled by anti-ARF1 antiserum (P–R). Note fluorescence and gold labeling on the identical section (P–T).

cw, cell wall; cp, cell plate; n, nucleus; v, vacuole. Scale bars, 20 μm (A and D); 10 μm (I, K, P, and Q); 1 μm (F, M, R, S, and T); 0.5 μm (N and O); and 0.25 μm (E, G, H, and L).

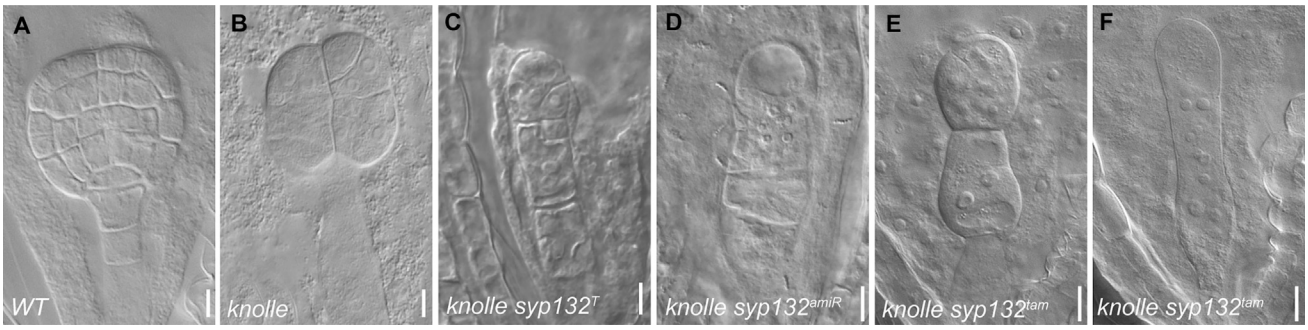

Figure 4. *syp132 Knolle* Double-Mutant Embryos Showing Strong Cytokinesis Defects

(A–F) Images of chloral hydrate-cleared whole-mount preparations of embryos. (A) Wild-type (WT); (B) *knolle* mutant; (C and D) *knolle syp132* double mutants: (C) *knolle syp132*^{T}; (D) *knolle syp132*^{amiR}; (E and F) *knolle syp132*^{tam}. Scale bars, 10 μm (A–F). See also Tables S1, S2, and S4.

nuclei (Figures 4E, 4F, and S2M–S2P; Table S1). These observations indicate that cytokinesis is almost completely abolished in the *knolle syp132*^{tam} double mutant from the zygote stage onward. The variability of the cytokinesis-defective phenotype can be attributed to the incomplete elimination of *SYP132* mRNA.

SNARE Interaction Partners of SYP132

To identify potential interaction partners of SYP132 among SNARE proteins, we investigated whether or not the knock out of individual KNOLLE partners enhanced the *knolle* knockout phenotype. If a KNOLLE partner also interacted with SYP132, double-mutant embryos lacking both KNOLLE and that specific SNARE protein would be expected to display a stronger mutant phenotype than *knolle* mutant embryos do on their own. In contrast, if that SNARE protein interacted with KNOLLE specifically, then no enhanced phenotype would be expected in the double mutant. We analyzed double-mutant embryos lacking KNOLLE and any one of its Qb-, Qc-, and Qbc-SNARE interaction partners: *knolle npsn11*, *knolle syp71*^{amiR}, and *knolle snap33*. For each combination, the double mutants died as embryos with an enhanced cytokinesis-defective phenotype: the embryos consisted of a few enlarged cells, sometimes with multiple nuclei, displaying cell-wall stubs (Figures 5A–5E, Tables S1, S2). This contrasted with the embryo viability of the single mutants (Heese et al., 2001; Zheng et al., 2002; El Kasmi et al., 2013). These results thus suggested that SNARE partners of KNOLLE might also be partners of SYP132.

To test for physical interaction between SYP132 and KNOLLE-interacting SNARE proteins, we performed co-immunoprecipitation experiments on protein extracts from transgenic plants expressing genomic *SYP132::GFP-SYP132* or *KNOLLE::Myc-SYP132* constructs. SYP132 did indeed interact with the SNARE partners of KNOLLE (Figures 5F and 5G). In the reciprocal experiment, the putative SNARE partners were immunoprecipitated, and each precipitate also contained both KNOLLE and SYP132 proteins (Figures 5H and 5I). In contrast, SNAP33 was not detected in the precipitates of YFP-NPSN11 and YFP-SYP71 (Figure 5H). Thus, like KNOLLE, SYP132 participated in two different complexes, since NPSN11 and SNAP33 had been shown before not to reside in the same KNOLLE complex (El Kasmi et al., 2013). One SYP132 complex contained the SNARE partners SNAP33 and VAMP721 or VAMP722, which cannot be distinguished with the antiserum available, whereas the other contained NPSN11 and SYP71 in addition to VAMP721 or VAMP722. These results indicate that the Qa-SNAREs SYP132 and KNOLLE each form complexes with the same SNARE partners to mediate membrane fusion in *Arabidopsis* cytokinesis.

Unlike KNOLLE, SYP132 Is Not Required for Endosperm Cellularization

The embryo-nourishing tissue called the endosperm originates together with the embryo through double fertilization; this is an evolutionary novelty of angiosperm reproduction (Floyd and Friedman, 2001; Friedman and Ryerson, 2009). Double fertilization involves two genetically identical haploid sperm cells, which each fertilize one of two genetically identical female gametes, the haploid egg cell and a diploid central cell, derived from the same meiotic product. In contrast to a series of cell divisions that transform the fertilized egg cell into a young embryo, the initial development of endosperm occurs within a large single cell, resembling *Drosophila* early embryogenesis: a series of nuclear division cycles is followed by the simultaneous formation of partitioning membranes that separate the many nuclei from each other, so-called cellularization (for review, see Mazumdar and Mazumdar, 2002). The Qa-SNARE KNOLLE is strongly expressed during endosperm cellularization and also during subsequent rounds of cytokinesis of the cellular endosperm (Figures 6A and 6C) (Day et al., 2008; Lauber et al., 1997). Furthermore, *knolle* mutant endosperm (almost) fails to cellularize, indicating that KNOLLE plays an essential role in endosperm development (Figure 6J, compare with 6I) (Sørensen et al., 2002). In contrast to KNOLLE, GFP-SYP132 was weakly and unevenly expressed in cellularizing endosperm, but subsequently accumulated strongly in the plasma membrane of endosperm cells (Figures 6B and 6D). To determine the functional requirement of SYP132 in the endosperm, the phenotype of *syp132*^{tam} developing embryo and endosperm within the same seed was analyzed. Although the *syp132*^{tam} mutant embryos displayed characteristic cytokinesis defects, resembling *knolle* mutant embryos, the associated endosperm essentially looked like wild-type, in contrast to the nearly complete elimination of endosperm cellularization in *knolle* mutants (Figure 6K, compare with 6I–6J). In conclusion, whereas KNOLLE is strictly required for endosperm cellularization SYP132 appears dispensable, although it plays an essential role in zygotic cytokinesis.

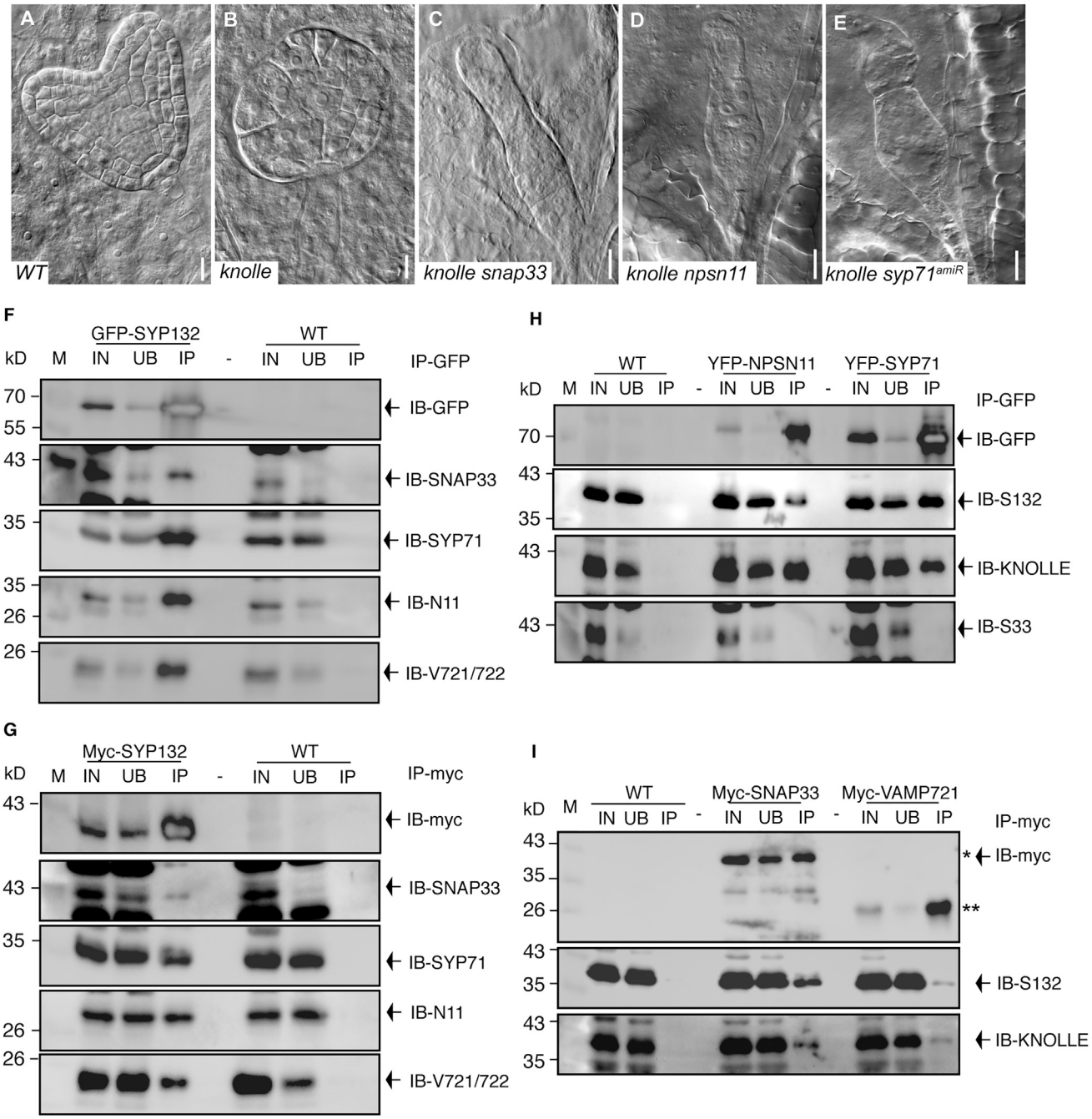

Figure 5. Genetic and Biochemical Interactions of SNAREs

(A–E) SNARE double-mutant embryos showing enhanced *knolle* mutant phenotypes. (A) Wild-type (WT); (B) *knolle* mutant; (C–E) double mutants of *knolle* and known KNOLLE-interacting Q-SNARE partners: (C) *knolle snap33*, (D) *knolle npsn11*, and (E) *knolle syp71*^{amiR}. Note that each double mutant shows more abnormal phenotype than each single mutant of *npsn11*, *snap33*, and *syp71*^{amiR}, which display no or only a slight cytokinesis phenotype (El Kasmi et al., 2013). Scale bars, 10 μm (A–E). See also Tables S1, S2, and S4.

(F–I) Co-immunoprecipitation analysis. Protein extracts from SYP132::GFP-SYP132 (F) and KNOLLE::Myc-SYP132 (G) seedlings were subjected to immunoprecipitation (IP) with anti-GFP and anti-Myc beads, respectively. (Col) was used as control. Immunoprecipitates were probed by immunoblotting (IB) for SNARE proteins NPSN11 (N11), SNAP33, SYP71, and VAMP721/722 (V721/722). (H and I) Reciprocal co-immunoprecipitation analysis. Protein extracts of YFP-NPSN11, middle in (H), or YFP-SYP71, right in (H), and Myc-SNAP33, left in (I), and Myc-VAMP721, right in (I) seedlings were subjected to IP with anti-GFP and anti-Myc beads, respectively. WT, left in (H) and (I) was used as control. Immunoprecipitates were probed by IB for Qa-SNAREs KNOLLE and SYP132 (S132), and for Qbc-SNAP33 (S33) in (H). Single asterisk (I) (upper panel), Myc-SNAP33; double asterisks (I) (upper panel), Myc-VAMP721. IN, input; UB, unbound; IP, immunoprecipitate. Molecular sizes (in kDa) are indicated on the left.

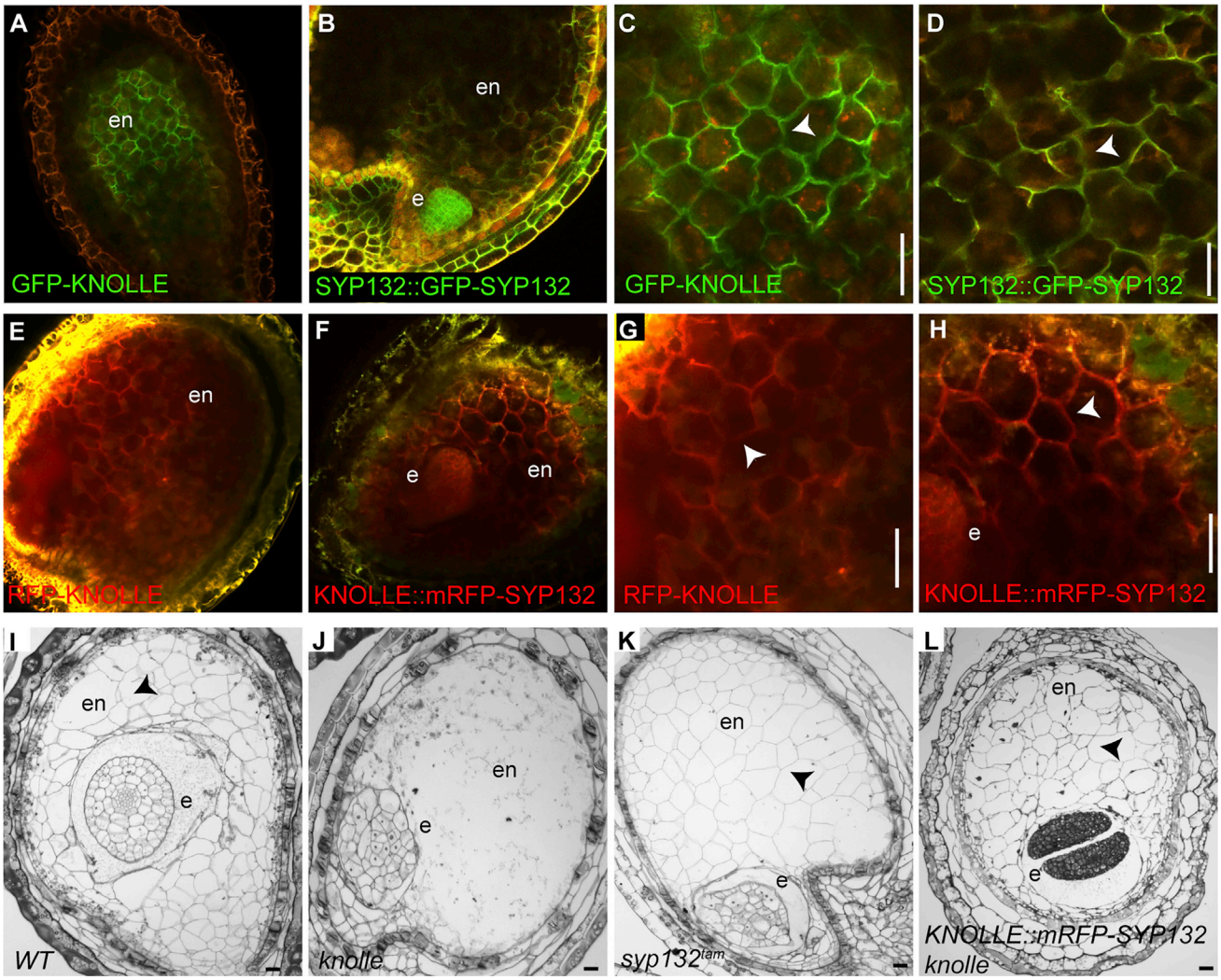

Figure 6. Qa-SNAREs SYP132 and KNOLLE in Endosperm Cellularization

(A–H) Localization of Qa-SNARE proteins in cellularizing endosperm: (A and C) KNOLLE::GFP-KNOLLE; (B and D) SYP132::GFP-SYP132; (E and G) KNOLLE::RFP-KNOLLE; (F and H) KNOLLE:mRFP-SYP132 *knolle*. (A, B, E, and F) Overviews. (C, D, G, and H) Highly magnified images taken from the peripheral endosperm at different or same focal planes. Note brightly stained embryo in (B and F). At the same detector setting, the GFP-KNOLLE signal was approximately 3-fold stronger than the GFP-SYP132 signal. In contrast, KNOLLE::mRFP-SYP132 expression was indistinguishable from KNOLLE::RFP-KNOLLE expression (E–H) (see also Figure S6 for immunofluorescent images and quantification analysis). Note that the counter colors, red in (A)–(D) and green in (E)–(H) represent an autofluorescent signal from the clearing.

(I–L) Endosperm in developing seeds of (I) WT (Col), (J) *knolle*, (K) *syp132*^{tam}, and (L) *KNOLLE::mRFP-SYP132 knolle*. Note the absence of cellular endosperm in *knolle* (J), but not in *syp132*^{tam} (K). In contrast, cellularization of the endosperm in *knolle* was rescued by *KNOLLE::mRFP-SYP132* (L), which resembled WT (I) and *syp132*^{tam} (K) ovules. Arrowheads indicate formation of partitioning membranes during cellularization (C, D, G, and H) and cell walls in cellular endosperm (I, K, and L). e, embryo derived from zygote; en, endosperm.

Scale bars, 20 μm (C, D, G, and H) and 10 μm (I–L). See also Tables S3 and S4.

To examine whether the differences in expression level might be responsible for the requirement of KNOLLE, as opposed to SYP132 in endosperm cellularization, we expressed SYP132 fused to mRFP from the *KNOLLE cis*-regulatory sequences in the *knolle* mutant background (Müller et al., 2003), which rescues the *knolle* mutant fully (Reichardt et al., 2011; Figure S5; Table S3). In the cellularizing endosperm, mRFP-SYP132 accumulated in midplane between adjacent nuclei, essentially like RFP-KNOLLE (Figures 6F and 6H, compare with 6E, 6G, and S6). Light microscopic analysis of sections of *KNOLLE::mRFP-SYP132 knolle* ovules revealed normal cellularization of the endosperm (Figure 6L). These results strongly suggest that the regulation of gene expression is the crucial feature of KNOLLE function in endosperm cellularization.

DISCUSSION

Our results suggest a plausible scenario for the evolution of membrane fusion during plant cytokinesis. The cytokinesis-specific Qa-SNARE KNOLLE is only conserved among flowering

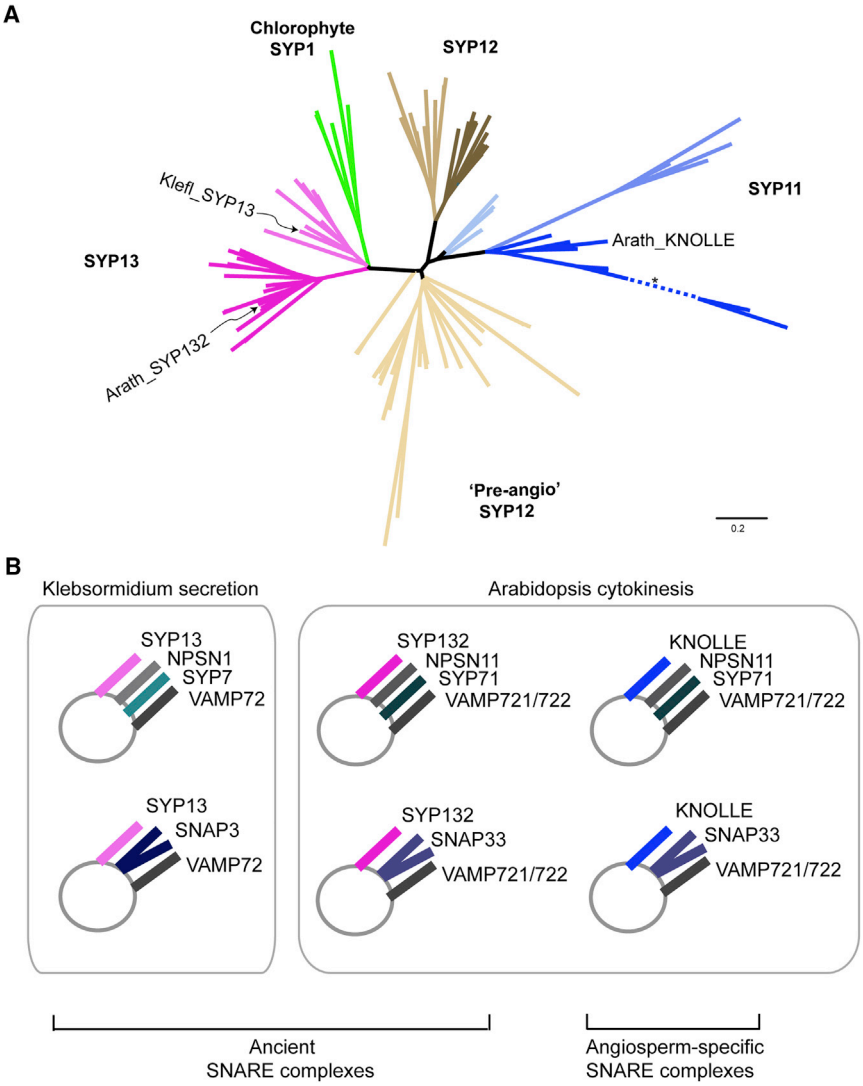

Figure 7. Evolution of Membrane Fusion in Plant Cytokinesis

(A) SYP1 phylogenetic tree (abridged). Proteins were aligned using MUSCLE in MEGA7. Phylogeny was generated using the Neighbor-Joining method in MEGA7. KNOLLE, SYP132 of *Arabidopsis thaliana* and SYP13 of *Klebsormidium flaccidum* are indicated. Note that the branch marked with an asterisk was shortened to 33%. See also Figure S7 for detailed phylogenetic tree.

(B) Model of SNARE complexes in cytokinesis. SYP132 complexes in *Arabidopsis* are evolutionarily ancient, resembling the putative secretory SYP13-containing SNARE complexes in the charophycean alga *Klebsormidium flaccidum* while KNOLLE complexes in *Arabidopsis* are angiosperm-specific SNARE complexes confined to cytokinesis.

plants (Figures 7A and S7), although the plant mode of phragmoplast-assisted cell-plate formation was already established in the charophycean algae that gave rise to the land plants (Doty et al., 2014; for review, see Buschmann and Zachgo, 2016). Unlike KNOLLE, SYP132 has counterparts in lower plants, starting in algae (Figures 7A and S7). In the sequenced genome of the charophycean alga *Klebsormidium flaccidum*, there are single-copy genes encoding putative SYP1 SNARE complex members (Hori et al., 2014): one SYP132-like Qa-SNARE (KfSYP13; kfl00435_0060; e-value, 4e-103), one SNAP33-like Qbc-SNARE (KfSNAP3; kfl00640_0070; e-value, 1e-42), one NPSN11-like Qb-SNARE (KfNPSN1; kfl00187_0180; e-value, 7e-93), one SYP71-like Qc-SNARE (KfSYP7; kfl00527_0090; e-value, 3e-95) and one VAMP721-like R-SNARE (KfVAMP72; kfl00515_0100; e-value, 7e-107). Taking into account the phylogenetic relationships between these proteins and their *Arabidopsis* counterparts as well as the interactions of the latter shown here, we propose that two different types of SYP1 SNARE complexes might already have existed in ancient algae giving rise to land plants: (1) SYP13-NPSN1-SYP7-VAMP72 and (2) SYP13-SNAP3-VAMP72 (Figure 7B). Those putative SNARE complexes would thus have involved the same single SYP1 Qa-SNARE related to SYP132 of *Arabidopsis* and the same single R-SNARE related to VAMP721 of *Arabidopsis*. Furthermore, those two complexes would have mediated membrane fusion both of secretory vesicles with the plasma membrane and of membrane vesicles with each other and the forming partitioning membrane during cytokinesis. Interestingly, *Klebsormidium* still displays centripetal furrowing as its prevalent mode of cytokinesis, thus superficially resembling the non-plant mode of cytokinesis, which is mediated by a contractile ring (Katsaros et al., 2011). Nonetheless, the only *SYP1* gene of *Klebsormidium* most closely relates to the *SYP13* clade of land plants, unlike the only *SYP1* gene of chlorophyte algae such as *Chlamydomonas*, which appears to be equally distantly related to SYP13 and SYP12 clades of plant SYP1 Qa-SNAREs (Kanazawa et al., 2016) (Figure S7).

Starting from the single SYP13 in *Klebsormidium*, the SYP1 family of Qa-SNAREs presumably evolved by gene duplication and diversification. A new branch of SYP12 members appears to have originated in the early land plants, as represented in the moss *Marchantia polymorpha* (Kanazawa et al., 2016) (Figure S7). Only much later was the SYP11 branch established. Although SYP11 proteins are encoded in the three gymnosperm genomes analyzed so far, they still appear different from the cytokinesis-specific KNOLLE protein of flowering plants, raising the possibility that KNOLLE-like proteins might only have acquired a novel essential role in angiosperms.

Although the charophycean algae established phragmoplast-assisted cell-plate formation as the plant-specific mode of cytokinesis several hundred million years ago, it appears that a cytokinesis-specific Qa-SNARE related to KNOLLE arose only with the advent of angiosperms. We propose that this led to

the formation of SNARE complexes specifically involved in cytokinesis and playing no role in secretory traffic to the plasma membrane during interphase. The primary mechanism of KNOLLE sub-functionalization most likely was the acquisition of paired *cis*-regulatory elements such as MSA sequences required for strong expression during the G2/M phase of the cell cycle (Haga et al., 2007), which presumably was accompanied by changes causing KNOLLE protein degradation at the end of cytokinesis. Although cytokinesis-specific SNARE complexes exist in *Arabidopsis*, and most likely in other flowering plants as well (see Müller et al., 2003), there is still a contribution of the ancient SYP132-containing SNARE complexes to cytokinesis, in addition to their role in secretion. These observations beg the question of why KNOLLE was selected for in the flowering plants and, conversely, why the ancient Qa-SNARE SYP132 was nonetheless retained. Our results indicate that SYP132 is absolutely required for secretion and also plays a role in cytokinesis during embryogenesis. Conversely, KNOLLE, but not SYP132, is necessary not only for somatic cytokinesis but also for the cellularization of the endosperm (compare Figures 6J with 6K). In endosperm cellularization, membrane vesicles are delivered to the midplane between adjacent nuclei, where they fuse with one another to form partitioning membranes, as in somatic cytokinesis (Otegui et al., 2001). Thus, the role of KNOLLE in endosperm cellularization is mechanistically akin to its role in somatic cytokinesis: promoting the fusion of membrane vesicles delivered to the midplane between adjacent nuclei by forming SNARE complexes to generate the partitioning membranes, which separate hundreds of nuclei from each other simultaneously. However, compared with somatic embryogenesis, endosperm cellularization has a much higher demand for membrane-fusion capacity, which appears to be met by the very strong G2/M-phase expression of KNOLLE. This conclusion is strongly supported by the observation that SYP132 expressed from a transgene with *KNOLLE cis*-regulatory sequences accumulated like KNOLLE in midplane between adjacent nuclei during endosperm cellularization and was sufficient to rescue the cellularization defect of *knolle* mutant endosperm. It is interesting to note that the endosperm, which is an extra-embryonic nourishing tissue for the embryo, is a peculiarity of angiosperms, resulting from the double-fertilization event unique to flowering plants. It is thus tempting to speculate that the origin of this evolutionary novelty was facilitated by the emergence of a cytokinesis-specific Qa-SNARE.

STAR★METHODS

Detailed methods are provided in the online version of this paper and include the following:

- KEY RESOURCES TABLE
- CONTACT FOR REAGENT AND RESOURCE SHARING
- METHOD DETAILS
  - Plant Material and Growth Conditions
  - TILLING
  - Molecular Cloning and Genetic Analysis
  - Immunoprecipitation
  - Immunofluorescence Imaging
  - Two-Photon Imaging of Cellularizing Endosperm
  - Electron Microscopy and CLEM
  - Phylogenetic Tree Generation
  - Phenotypic Analysis

SUPPLEMENTAL INFORMATION

Supplemental Information includes seven figures and four tables and can be found with this article online at https://doi.org/10.1016/j.devcel.2017.12.027.

ACKNOWLEDGMENTS

We thank Franziska Birkhold, Rebecca Stahl, and Lorenz Henneberg for technical assistance, Natasha V. Raikhel for providing rabbit anti-NPSN11 antiserum, and the ABRC and NASC Stock Centers for plant material. We thank Niko Geldner, Maren Heese, and Thorsten Nürnberger for critical discussion. This work was supported by grants Ju 179/19-1 and SFB 1101 (to Y.-D.S.) from the Deutsche Forschungsgemeinschaft.

AUTHOR CONTRIBUTIONS

Investigation, Validation, Writing – Review & Editing, and Visualization, M.P.; Investigation, C.K., M. Karnahl, I.R., F.E.K., U.M., Y.-D.S., U.H., M.B., and M. Kientz; Resources, M.H.S., M.T.N., and J.L.D.; Resources and Investigation, A.A.S.; Conceptualization, Supervision, Project Administration, Writing – Original Draft Preparation, Writing – Review & Editing, and Funding Acquisition, G.J.

DECLARATION OF INTERESTS

The authors declare no competing interests.

Received: June 10, 2017
Revised: November 29, 2017
Accepted: December 28, 2017
Published: January 25, 2018

REFERENCES

Assaad, F.F., Huet, Y., Mayer, U., and Jürgens, G. (2001). The cytokinesis gene KEULE encodes a Sec1 protein that binds the syntaxin KNOLLE. J. Cell Biol. *152*, 531–543.

Buschmann, H., and Zachgo, S. (2016). The evolution of cell division: from streptophyte algae to land plants. Trends Plant Sci. *21*, 872–883.

Catalano, C.M., Czymmek, K.J., Gann, J.G., and Sherrier, D.J. (2007). *Medicago truncatula* syntaxin SYP132 defines the symbiosome membrane and infection droplet membrane in root nodules. Planta *225*, 541–550.

Clough, S.J., and Bent, A.F. (1998). Floral dip: a simplified method for Agrobacterium-mediated transformation of *Arabidopsis thaliana*. Plant J. *16*, 735–743.

Collins, N.C., Thordal-Christensen, H., Lipka, V., Bau, S., Kombrink, E., Qiu, J.L., Hückelhoven, R., Stein, M., Freialdenhoven, A., Somerville, S.C., et al. (2003). SNARE-protein-mediated disease resistance at the plant cell wall. Nature *425*, 973–977.

Cook, M.E. (2004). Cytokinesis in *Coleochaete orbicularis* (Charophyceae): an ancestral mechanism inherited by plants. Am. J. Bot. *91*, 313–320.

Day, R.C., Herridge, R.P., Ambrose, B.A., and Macknight, R.C. (2008). Transcriptome analysis of proliferating *Arabidopsis* endosperm reveals biological implications for the control of syncytial division, cytokinin signaling, and gene expression regulation. Plant Physiol. *148*, 1964–1984.

Doty, K.F., Betzelberger, A.M., Kocot, K.M., and Cook, M.E. (2014). Immunofluorescence localization of the tubulin cytoskeleton during cell division and cell growth in members of the Coleochaetales (Streptophyta). J. Phycol. *50*, 624–639.

El Kasmi, F., Krause, C., Hiller, U., Stierhof, Y., Mayer, U., Conner, L., Kong, L., Reichardt, I., Sanderfoot, A., and Jürgens, G. (2013). SNARE complexes of

different composition jointly mediate membrane fusion in *Arabidopsis* cytokinesis. Mol. Biol. Cell *24*, 1593–1601.

Enami, K., Ichikawa, M., Uemura, T., Kutsuna, N., Hasezawa, S., Nakagawa, T., Nakano, A., and Sato, M.H. (2009). Differential expression control and polarized distribution of plasma membrane-resident SYP1 SNAREs in *Arabidopsis thaliana*. Plant Cell Physiol. *50*, 280–289.

Felsenstein, J. (1985). Confidence limits on phylogenies: an approach using the bootstrap. Evolution *39*, 783–791.

Floyd, S., and Friedman, W. (2001). Developmental evolution of endosperm in basal angiosperms: evidence from *Amborella* (Amborellaceae), *Nuphar* (Nymphaeaceae), and *Illicium* (Illiciaceae). Plant Syst. Evol. *228*, 153–169.

Friedman, W., and Ryerson, K. (2009). Reconstructing the ancient female gametophyte in angiosperms: insights from *Amborella* and other ancient lineages of flowering plants. Am. J. Bot. *96*, 129–143.

Fujiwara, M., Uemura, T., Ebine, K., Nishimori, Y., Ueda, T., Nakano, A., Sato, M.H., and Fukao, Y. (2014). Interactomics of Qa-SNARE in *Arabidopsis thaliana*. Plant Cell Physiol. *55*, 781–789.

Grefen, C., Chen, Z., Honsbein, A., Donald, N., Hills, A., and Blatt, M.R. (2010). A novel motif essential for SNARE interaction with the K(+) channel KC1 and channel gating in *Arabidopsis*. Plant Cell *22*, 3076–3092.

Gromley, A., Yeaman, C., Rosa, J., Redick, S., Chen, C.T., Mirabelle, S., Guha, M., Sillibourne, J., and Doxsey, S.J. (2005). Centriolin anchoring of exocyst and SNARE complexes at the midbody is required for secretory-vesicle-mediated abscission. Cell *123*, 75–87.

Haga, N., Kato, K., Murase, M., Araki, S., Kubo, M., Demura, T., Suzuki, K., Müller, I., Voss, U., Jürgens, G., et al. (2007). R1R2R3-Myb proteins positively regulate cytokinesis through activation of KNOLLE transcription in *Arabidopsis thaliana*. Development *134*, 1101–1110.

Hedges, S.B., Blair, J.E., Venturi, M.L., and Shoe, J.L. (2004). A molecular timescale of eukaryote evolution and the rise of complex multicellular life. BMC Evol. Biol. *4*, 2.

Heese, M., Gansel, X., Sticher, L., Wick, P., Grebe, M., Granier, F., and Jürgens, G. (2001). Functional characterization of the KNOLLE-interacting t-SNARE AtSNAP33 and its role in plant cytokinesis. J. Cell Biol. *155*, 239–249.

Hori, K., Maruyama, F., Fujisawa, T., Togashi, T., Yamamoto, N., Seo, M., Sato, S., Yamada, T., Mori, H., Tajima, N., et al. (2014). *Klebsormidium flaccidum* genome reveals primary factors for plant terrestrial adaptation. Nat. Commun. *5*, 3978.

Huisman, R., Hontelez, J., Mysore, K.S., Wen, J., Bisseling, T., and Limpens, E. (2016). A symbiosis-dedicated SYNTAXIN OF PLANTS 13II isoform controls the formation of a stable host-microbe interface in symbiosis. New Phytol. *211*, 1338–1351.

Ichikawa, M., Hirano, T., Enami, K., Fuselier, T., Kato, N., Kwon, C., Voigt, B., Schulze-Lefert, P., Baluška, F., and Sato, M.H. (2014). Syntaxin of plant proteins SYP123 and SYP132 mediate root hair tip growth in *Arabidopsis thaliana*. Plant Cell Physiol. *55*, 790–800.

Kalde, M., Nühse, T., Findlay, K., and Peck, S. (2007). The syntaxin SYP132 contributes to plant resistance against bacteria and secretion of pathogenesis-related protein 1. Proc. Natl. Acad. Sci. USA *104*, 11850–11855.

Kanazawa, T., Era, A., Minamino, N., Shikano, Y., Fujimoto, M., Uemura, T., Nishihama, R., Yamato, K.T., Ishizaki, K., Nishiyama, T., et al. (2016). SNARE molecules in *Marchantia polymorpha*: unique and conserved features of the membrane fusion machinery. Plant Cell Physiol. *57*, 307–324.

Katsaros, C., Varvarigos, V., Gachon, C.M., Brand, J., Motomura, T., Nagasato, C., and Küpper, F.C. (2011). Comparative immunofluorescence and ultrastructural analysis of microtubule organization in *Uronema* sp., *Klebsormidium flaccidum*, *K. subtilissimum*, *Stichococcus bacillaris* and *S. chloranthus* (Chlorophyta). Protist *162*, 315–331.

Kumar, S., Stecher, G., and Tamura, K. (2016). MEGA7: molecular evolutionary genetics analysis version 7.0 for bigger datasets. Mol. Biol. Evol. *33*, 1870–1874.

Kwon, C., Neu, C., Pajonk, S., Yun, H.S., Lipka, U., Humphry, M., Bau, S., Straus, M., Kwaaitaal, M., Rampelt, H., et al. (2008). Co-option of a default secretory pathway for plant immune responses. Nature *451*, 835–840.

Lauber, M.H., Waizenegger, I., Steinmann, T., Schwarz, H., Mayer, U., Hwang, I., Lukowitz, W., and Jürgens, G. (1997). The *Arabidopsis* KNOLLE protein is a cytokinesis-specific syntaxin. J. Cell Biol. *139*, 1485–1493.

Limpens, E., Ivanov, S., van Esse, W., Voets, G., Fedorova, E., and Bisseling, T. (2009). Medicago N2-fixing symbiosomes acquire the endocytic identity marker Rab7 but delay the acquisition of vacuolar identity. Plant Cell *21*, 2811–2828.

Low, S., Li, X., Miura, M., Kudo, N., Quiñones, B., and Weimbs, T. (2003). Syntaxin 2 and endobrevin are required for the terminal step of cytokinesis in mammalian cells. Dev. Cell *4*, 753–759.

Lukowitz, W., Mayer, U., and Jürgens, G. (1996). Cytokinesis in the *Arabidopsis* embryo involves the syntaxin-related KNOLLE gene product. Cell *84*, 61–71.

Mazumdar, A., and Mazumdar, M. (2002). How one becomes many: blastoderm cellularization in *Drosophila melanogaster*. Bioessays *24*, 1012–1022.

McCallum, C.M., Comai, L., Greene, E.A., and Henikoff, S. (2000). Targeting induced local lesions in genomes (TILLING) for plant functional genomics. Plant Physiol. *123*, 439–442.

Mierzwa, B., and Gerlich, D. (2014). Cytokinetic abscission: molecular mechanisms and temporal control. Dev. Cell *31*, 525–538.

Müller, I., Wagner, W., Völker, A., Schellmann, S., Nacry, P., Küttner, F., Schwarz-Sommer, Z., Mayer, U., and Jürgens, G. (2003). Syntaxin specificity of cytokinesis in *Arabidopsis*. Nat. Cell Biol. *5*, 531–534.

Musielak, T.J., Slane, D., Liebig, C., and Bayer, M. (2016). A versatile optical clearing protocol for deep tissue imaging of fluorescent proteins in *Arabidopsis thaliana*. PLoS One *11*, e0161107.

Nakayama, K. (2016). Regulation of cytokinesis by membrane trafficking involving small GTPases and the ESCRT machinery. Crit. Rev. Biochem. Mol. Biol. *51*, 1–6.

Otegui, M.S., Mastronarde, D.N., Kang, B.H., Bednarek, S.Y., and Staehelin, L.A. (2001). Three-dimensional analysis of syncytial-type cell plates during endosperm cellularization visualized by high resolution electron tomography. Plant Cell *13*, 2033–2051.

Pan, H., Oztas, O., Zhang, X., Wu, X., Stonoha, C., Wang, E., Wang, B., and Wang, D. (2016). A symbiotic SNARE protein generated by alternative termination of transcription. Nat. Plants *2*, 15197.

Park, M., Touihri, S., Müller, I., Mayer, U., and Jürgens, G. (2012). Sec1/Munc18 protein stabilizes fusion-competent syntaxin for membrane fusion in *Arabidopsis* cytokinesis. Dev. Cell *22*, 989–1000.

Reichardt, I., Slane, D., El Kasmi, F., Knöll, C., Fuchs, R., Mayer, U., Lipka, V., and Jürgens, G. (2011). Mechanisms of functional specificity among plasma-membrane syntaxins in *Arabidopsis*. Traffic *12*, 1269–1280.

Reichardt, I., Stierhof, Y., Mayer, U., Richter, S., Schwarz, H., Schumacher, K., and Jürgens, G. (2007). Plant cytokinesis requires de novo secretory trafficking but not endocytosis. Curr. Biol. *17*, 2047–2053.

Richter, S., Kientz, M., Brumm, S., Nielsen, M., Park, M., Gavidia, R., Krause, C., Voss, U., Beckmann, H., Mayer, U., et al. (2014). Delivery of endocytosed proteins to the cell-division plane requires change of pathway from recycling to secretion. Elife *8*, e02131.

Saitou, N., and Nei, M. (1987). The neighbor-joining method: a new method for reconstructing phylogenetic trees. Mol. Biol. Evol. *4*, 406–425.

Sanderfoot, A.A., Kovaleva, V., Bassham, D.C., and Raikhel, N.V. (2001). Interactions between syntaxins identify at least five SNARE complexes within the Golgi/prevacuolar system of the *Arabidopsis* cell. Mol. Biol. Cell *12*, 3733–3743.

Sanderfoot, A. (2007). Increases in the number of SNARE genes parallels the rise of multicellularity among the green plants. Plant Physiol. *144*, 6–17.

Sawitzky, H., and Grolig, F. (1995). Phragmoplast of the green alga *Spirogyra* is functionally distinct from the higher plant phragmoplast. J. Cell Biol. *130*, 1359–1371.

Schiel, J.A., and Prekeris, R. (2013). Membrane dynamics during cytokinesis. Curr. Opin. Cell Biol. *25*, 92–98.

Schmid, M., Davison, T.S., Henz, S.R., Pape, U.J., Demar, M., Vingron, M., Schölkopf, B., Weigel, D., and Lohmann, J.U. (2005). A gene expression map of *Arabidopsis thaliana* development. Nat. Genet. *37*, 501–506.

Schwab, R., Ossowski, S., Riester, M., Warthmann, N., and Weigel, D. (2006). Highly specific gene silencing by artificial microRNAs in *Arabidopsis*. Plant Cell *18*, 1121–1133.

Sørensen, M., Mayer, U., Lukowitz, W., Robert, H., Chambrier, P., Jürgens, G., Somerville, C., Lepiniec, L., and Berger, F. (2002). Cellularisation in the endosperm of *Arabidopsis thaliana* is coupled to mitosis and shares multiple components with cytokinesis. Development *129*, 5567–5576.

Staehelin, L.A., and Hepler, P.K. (1996). Cytokinesis in higher plants. Cell *84*, 821–824.

Stierhof, Y.D., and El Kasmi, F. (2010). Strategies to improve the antigenicity, ultrastructure preservation and visibility of trafficking compartments in *Arabidopsis* tissue. Eur. J. Cell Biol. *89*, 285–297.

Suwastika, I., Uemura, T., Shiina, T., Sato, M., and Takeyasu, K. (2008). SYP71, a plant-specific Qc-SNARE protein, reveals dual localization to the plasma membrane and the endoplasmic reticulum in *Arabidopsis*. Cell. Struct. Funct. *33*, 185–192.

Till, B.J., Reynolds, S.H., Greene, E.A., Codomo, C.A., Enns, L.C., Johnson, J.E., Burtner, C., Odden, A.R., Young, K., Taylor, N.E., et al. (2003). Large-scale discovery of induced point mutations with high-throughput TILLING. Genome Res. *13*, 524–530.

Waizenegger, I., Lukowitz, W., Assaad, F., Schwarz, H., Jürgens, G., and Mayer, U. (2000). The *Arabidopsis* KNOLLE and KEULE genes interact to promote vesicle fusion during cytokinesis. Curr. Biol. *10*, 1371–1374.

Wang, X., Wang, X., Deng, L., Chang, H., Dubcovsky, J., Feng, H., Han, Q., Huang, L., and Kang, Z. (2014). Wheat TaNPSN SNARE homologues are involved in vesicle-mediated resistance to stripe rust (*Puccinia striiformis* f. sp. *tritici*). J. Exp. Bot. *65*, 4807–4820.

Weijers, D., Van Hamburg, J.P., Van Rijn, E., Hooykaas, P.J., and Offringa, R. (2003). Diphtheria toxin-mediated cell ablation reveals interregional communication during *Arabidopsis* seed development. Plant Physiol. *133*, 1882–1892.

Yoon, H.S., Hackett, J.D., Ciniglia, C., Pinto, G., and Bhattacharya, D. (2004). A molecular timeline for the origin of photosynthetic eukaryotes. Mol. Biol. Evol. *21*, 809–818.

Yun, H.S., Kwaaitaal, M., Kato, N., Yi, C., Park, S., Sato, M.H., Schulze-Lefert, P., and Kwon, C. (2013). Requirement of vesicle-associated membrane protein 721 and 722 for sustained growth during immune responses in *Arabidopsis*. Mol. Cells *35*, 481–488.

Zhang, G.F., and Staehelin, L.A. (1992). Functional compartmentation of the Golgi apparatus of plant cells: immunocytochemical analysis of high-pressure frozen- and freeze-substituted sycamore maple suspension culture cells. Plant Physiol. *99*, 1070–1083.

Zheng, H., Bednarek, S.Y., Sanderfoot, A.A., Alonso, J., Ecker, J.R., and Raikhel, N.V. (2002). NPSN11 is a cell plate-associated SNARE protein that interacts with the syntaxin KNOLLE. Plant Physiol. *129*, 530–539.

Zuckerkandl, E., and Pauling, L. (1965). Evolutionary divergence and convergence in proteins. In Evolving Genes and Proteins, V. Bryson and H.J. Vogel, eds. (Academic Press), pp. 97–166.

STAR★METHODS

KEY RESOURCES TABLE

REAGENT or RESOURCES	SOURCE	IDENTIFIER
Antibodies		
Rabbit anti-KNOLLE	Lauber et al., 1997	N/A
Rabbit anti-SYP132	This paper	N/A
Rabbit anti-SNAP33	Heese et al., 2001	N/A
Rabbit anti-NPSN11	Zheng et al., 2002	N/A
Rabbit anti-SYP71	Sanderfoot et al., 2001	N/A
Rabbit anti-VAMP721/722	Kwon et al., 2008	N/A
Mouse anti-GFP	Roche	RRID: AB_390913
Rat anti-RFP	Chromotek	RRID: AB_2336064
Mouse anti-Myc 9E10	Millipore	RRID: AB_309725
Goat anti-rabbit IgG-POD	Millipore	Cat#AP307P
Goat anti-mouse IgG-POD	Sigma-Aldrich	Cat#A2554
Goat anti-rat IgG-POD	Sigma-Aldrich	Cat#A9037
Goat anti-rabbit Alexa488	Invitrogen	Cat#A11008
Goat anti-rabbit Cy3™	Dianova	Cat#111-165-144
Goat anti-rat Cy3	Dianova	Cat#112-165-062
Goat anti-mouse IgG-Cy3	Dianova	Cat#115-165-062
Goat anti-mouse IgG-Gold	Dianova	Cat#115-195-166
Mouse anti-Xyloglucan	Zhang and Staehelin, 1992	N/A
Anti-GFP agarose	Chromotek	RRID: AB_2631360
Anti-Myc agarose	Sigma-Aldrich	Cat#A7470
EDTA-free protease inhibitor cocktail	Roche	Cat#04693132001
Bacterial and Virus Strains		
Agrobacterium tumefaciens	ATCC	NCBITaxon:357
Chemicals, Peptides, and Recombinant Proteins		
DAPI	Sigma-Aldrich	Cat#D9542
FM4-64	Invitrogen	Cat#F34653; CHEBI-52078
BASTA	AgrEvo	N/A
LR-White Resin	Fluka	Cat#62662
EPON	Roth	Cat#8619
*Sma*I	Thermo Fischer scientific	Cat#ER0661
*EcoR*I	Thermo Fischer scientific	Cat#ER0271
Phusion Taq polymerase	Thermo Fischer scientific	Cat#F530L
Experimental Model: Organism		
Arabidopsis thaliana	NASC	NCBITaxon::3702
Plant Materials		
knolle$^{X37\text{-}2}$ mutant	Lukowitz et al., 1996	N/A
syp132^{T} mutant	This paper	N/A
syp132^{amiR} mutant	This paper	N/A
snap33 mutant	Heese et al., 2001	N/A
syp71^{amiR} mutant	El Kasmi et al., 2013	N/A
npsn11 mutant	Zheng et al., 2002	N/A
KNOLLE::Myc-SYP132	Reichardt et al., 2011	N/A
SYP132::GFP-SYP132	Enami et al., 2009	N/A
SNAP33::Myc-SNAP33	Heese et al., 2001	N/A

(*Continued on next page*)

Continued

REAGENT or RESOURCES	SOURCE	IDENTIFIER
KNOLLE::YFP-NPSN11	El Kasmi et al., 2013	N/A
SYP71::YFP-SYP71	Suwastika et al., 2008	N/A
RPS5A::GAL4	Weijers et al., 2003	N/A
KNOLLE::vYFP-SYP132_SYP123	This paper	N/A
KNOLLE::mRFP-SYP132	This paper	N/A
Recombinant DNAs		
KNOLLE expression cassette	Müller et al., 2003	N/A
KNOLLE::vYFP-SYP132_SYP123	This paper	N/A
KNOLLE::mRFP-SYP132	This paper	N/A
Oligonucleotides		
amiR(SYP132) targeting sequence: AGCACAGGTAATGGACACCT	This paper	N/A
Primers for genotyping mutants	See Table S4	N/A
Primers for recombinant DNAs construction	See Table S4	N/A
Primers for genotyping transgenes	See Table S4	N/A
Other		
Chemiluminescence detection system	PEQlab	Fusion Fx7 Imager
Immunohistochemistry system	Intavis	InsituPro VSi
Confocal laser scanning microscope	Leica	SP8
Two-photon laser scanning microscope	Zeiss	LSM780NLO
Cryomicrotome	Supercut	Leica RM2065
Electron microscope	Jeol	TEM

CONTACT FOR REAGENT AND RESOURCE SHARING

Further information and requests for reagents and resources should be directed to and will be fulfilled by the Lead Contact, Gerd Jürgens (gerd.juergens@zmbp.uni-tuebingen.de).

METHOD DETAILS

Plant Material and Growth Conditions

Arabidopsis thaliana genotypes used were wild-type (*Col-0*), *knolle*$^{X37\text{-}2}$ (*Ler/Nd*) (Lukowitz et al., 1996) and *snap33* (*Ws*) (Heese et al., 2001). In addition, T-DNA insertion lines were analyzed by PCR genotyping to identify homozygous *npsn11* (At2g35190; SALK_068094) and *syp132*^{T} (At5g08080, SAIL 403_B09) mutants. The following transgenic plant lines were used: *SYP132::GFP-SYP132* (Enami et al., 2009), *KNOLLE::Myc-SYP132* (Reichardt et al., 2011), *SNAP33::Myc-SNAP33* (Heese et al., 2001), *KNOLLE::YFP-NPSN11* (El Kasmi et al., 2013), *SYP71::YFP-SYP71* (Suwastika et al., 2008).

Plants were either grown on soil or on vertically oriented agar plates with 2.15 g/l Murashige and Skoog (1/2 MS) medium containing 1% sucrose in growth chambers at 23°C in continuous light. Transgenic plants were generated by transformation with *Agrobacterium tumefaciens* using the floral-dip method (Clough and Bent, 1998).

The homozygous *RPS5A::GAL4* activator line was transformed with *Agrobacterium* carrying *KNOLLE::vYFP-SYP132_SYP123.* T1 plants selected by spraying with 1:1000 diluted BASTA (183 g/l glufosinate; AgrEvo, Düsseldorf, Germany) were crossed with the homozygous *UAS::amiR(SYP132)* line. The resulting F1 was analysed for complementation test.

TILLING

Targeting induced local lesions in genomes (TILLING) of *SYP132* was performed as reported (McCallum et al. 2000). This approach is based on mismatch-specific endonuclease cleavage of heteroduplex DNA fragments formed upon PCR amplification of target gene sequences of individuals from a mutant population. To identify point mutations in *SYP132*, approximately 1500 M2 individuals from the ethyl methanesulfonat (EMS)-mutagenized population of *A. thaliana* (Col) were screened using two gene-specific primer pairs listed in Table S4. Seven mutations were identified in the *SYP132* gene: C2335T, C2363T and C2382T mutations in the introns; G2020A, G2221A and G2429A mutations in the exons. Of these, three mutations in the exons giving rise to point mutations (See Figure S1A for sequence comparison) were further analyzed. Seeds of lines carrying mutations in *SYP132* were obtained from the GABI-TILL Arabidopsis collection and screened twice independently.

Molecular Cloning and Genetic Analysis

Cloning of artificial microRNA (amiRNA) for SYP132 was done as described in Artificial microRNA Designer (http://wmd3.weigelworld.org/cgi-bin/webapp.cgi), using the primers listed in Table S4 (Schwab et al., 2006). For the two-component expression system, the amiRNA was cloned under the GAL4-responsive *UAS* element and these reporter lines were crossed with the *RPS5A::GAL4* activator lines (Weijers et al., 2003). The amino acid exchanges R218H and D238N were introduced into *KNOLLE* by site directed mutagenesis of *KNOLLE::Myc-KNOLLE*. The constructs were transformed in *knolle*$^{X37\text{-}2}$ heterozygous plants.

For *KNOLLE::vYFP-SYP132_SYP123*, a chimeric construct of *SYP132_SYP123* was generated with a primer-extension method. PCR product was digested with *Sma*I and *Eco*RI and subcloned in-frame downstream of *pKNOLLE::vYFP* cassette. For *KNOLLE::mRFP-SYP132*, *SYP132* was amplified by PCR using primers 132-start Sma1 and 132-stop EcoRI and subcloned in-frame downstream of *pKNOLLE::mRFP* cassette (*Sma*I/*Eco*RI). Genotyping PCR: X37-2 CIII and X37-2 DIII for *knolle* $^{X37\text{-}2}$ and *KNOLLE* (0. 5 kb and 1.5 kb, respectively); UASs and eGFP200rev for *syp132*^{amiR} (0.4 kb); GALs and GALas for *GAL4* (0.7 kb); vYFP700sen and 132-stop EcoR1 for *vYFP-SYP132_SYP123* (1.2 kb); mRFP700sen and 132-stop EcoR1 for *mRFP-SYP132* (1.2 kb). See Table S4 for primer sequences.

Immunoprecipitation

The immunoprecipitation procedure was modified from the previous report (Park et al., 2012). Total protein extracts were prepared from approximately 2 g of five-day-old seedlings in buffer (50 mM Tris pH7.5, 150 mM NaCl, 1 mM EDTA, 0.5% Triton X-100) supplemented with EDTA-free protease inhibitor cocktail (Roche). 30 μl of agarose-conjugated lama anti-GFP (GFP-trap®; Chromotek) or anti-Myc (Anti-c-Myc agarose affinity gel, Sigma-Aldrich) were added to cleared protein extract and incubated at 4°C for 2 h on a rolling incubator. All immunoprecipitation experiments were repeated more than twice. Membranes were developed using a chemiluminescence detection system (Fusion Fx7 Imager, PEQlab, Erlangen, Germany). Antibody dilutions were as follows: rabbit anti-KNOLLE serum (1:5,000) (Lauber et al., 1997), rabbit anti-SYP132 serum (1:5,000) (a kind gift from A. Sanderfoot), rabbit anti-SNAP33 serum (1:5,000) (Heese et al., 2001), rabbit anti-NPSN11 serum (1:1,500) (Zheng et al., 2002), rabbit anti-SYP71 serum (1:2,000) (Sanderfoot et al., 2001), rabbit anti-VAMP721/722 serum (1:5000) (Kwon et al., 2008), mouse anti-GFP monoclonal antibody (1:1,000; Roche), mouse anti-Myc monoclonal antibody 9E10 (1:1,000; Millipore), rat anti-RFP monoclonal antibody (1:1000; Chromotek), goat anti-rabbit IgG-POD polyclonal antibody (1:10,000; Millipore), goat anti-mouse IgG-POD polyclonal antibody (1:10,000; Sigma), goat anti-rat IgG-POD polyclonal antibody (1:5,000; Sigma).

Immunofluorescence Imaging

Live imaging in roots of five-day-old seedlings was performed with 2 μM FM4-64 (Molecular Probes, Life Technologies) in liquid growth medium (1/2 MS medium, 1% sucrose, pH 5.6). Five-day-old seedlings were fixed in 4% (w/v) paraformaldehyde in MTSB (50 mM Pipes, 5 mM EGTA, 5 mM $MgSO_4$, pH 7.0) for 1 hr and stored at -20°C until used for immunostaining. For embryo and endosperm staining, ovules fixed in 4% paraformaldehyde in MTSB were squashed on the gelatin-coated slide (Lauber et al., 1997). For immunofluorescence, primary antisera anti-KNOLLE (1:4000, rabbit) (Lauber et al., 1997), mouse anti-Myc monoclonal antibody 9E10 (1:600; Millipore), rat anti-RFP monoclonal antibody (1:500; Chromotek), goat anti-rabbit Alexa488 (1:600, Invitrogen), goat anti-rat Cy3 (1:600; Dianova), and goat anti-rabbit Cy3^{TM} (1:600, Dianova, Germany) were applied. PBS (pH 7.5) was used in all steps after fixation of the plant material. The primary antibody was incubated for 6 hours at 37°C after blocking for 3 hour with 3% BSA in PBS, the secondary antibody was incubated for 4 hours at 37°C. 1 μg/ml DAPI (1 mg/ml stock solution in H_2O) was used for staining nuclei. Samples were prepared manually or with an immunohistochemistry system (InsituPro VSi, Intavis, Cologne, Germany). Fluorescent images were taken using a 63x water-immersion objective in Leica SP8 confocal laser scanning microscope. Intensity profile was measured using Leica software. Images were processed with Adobe Photoshop CS3 only for adjustment of contrast and brightness.

Two-Photon Imaging of Cellularizing Endosperm

Experimental procedure was done as previously reported (Musielak et al., 2016). For whole-mount imaging of developing endosperm, immature seed of appropriate stage were dissected out of siliques and fixated in 4% paraformaldehyde in PBS buffer pH7.4 overnight at 4°C. After washing twice with water, the fixated ovules where cleared overnight and mounted in 50% thiodiethanol. Multi-photon imaging was performed with a Zeiss LSM780NLO equipped with a two-channel non-descanned GaAsP detector and a MaiTai DeepSee eHP IR laser. Excitation wavelength: GFP, 930 nm; mRFP, 745 nm; RFP, 755 nm. Images were taken with a Zeiss LD C-Apochromat 40x/1,1 W Korr objective.

Electron Microscopy and CLEM

For ultrastructural analysis, ovules were high-pressure frozen (HPM010) in 150 or 200 μm planchettes filled with hexadecane and freeze-substituted in acetone supplemented with 2.5% osmium tetroxide (35 h at -90°C, 6 h at -60°C, 6 h at -30°C, 2 h at 0°C). Thereafter samples were washed 5x with acetone (0°C), before they were infiltrated with 10%, 25%, 50%, 75%, 2x 100% epoxy resin (Roth, Germany). Infiltrated samples were polymerized at 60°C for two days. For ultrastructural analysis, 70 nm thin sections were cut and mounted on slot grids covered with pioloform. Sections were stained with 3% uranyl acetate in ethanol, followed by lead citrate and viewed in a Jeol JEM-1400plus TEM at 120 kV accelerating voltage. Images were taken with a 4K CMOS TemCam-F416 camera (TVIPS).

For resin section labeling with Xyloglucan-specific antibodies, ovules were high-pressure frozen as described above and freeze-substituted in acetone supplemented with 0.4% uranyl acetate and 1.6% methanol. After 50 h at -90°C, samples were warmed up to -50°C and washed 5x with acetone before they were infiltrated with 25%, 50%, 75% and 2x 100% Lowicryl HM20 at -50°C. Infiltrated samples were UV-polymerized for two days at -50°C. For immunolabeling, 70 nm thin sections were cut (Leica UC7) and mounted on coverslips for immunofluorescence microscopy or slot grids covered with Pioloform for immunoelectron microscopy and correlative light and electron microscopy (CLEM). For immunogold labeling of mounted sections on grids, unspecific binding sites were blocked with PBS containing 0.2% BSA and 0.2% milk powder. Sections were labeled as with mouse anti-xyloglucan antibodies (mAb CCRC-M1, 1:10; Carbosource Services, University of Gorgia) diluted in blocking buffer and goat anti-mouse IgG coupled to 6 nm gold (1:30; Dianova, Hamburg). In some cases, gold particles were silver-enhanced using R-Gent (Aurion, Wageningen) for 35-40 min. Resin sections were stained with 1% aqueous uranyl acetate for 4-5 min and lead citrate for 15-20 sec. For fluorescence labeling of coverslips, sections were labeled as described above with mouse anti-Xyloglucan antibodies (1:10) and goat anti-mouse IgG coupled to Cy3 (1:400; Dianova, Hamburg). Resin sections were stained for DNA with 1 μg/ml DAPI (4',6-diamidino-2-phenylindole) for 5 min and embedded in Moviol containing DABCO (1,4-diazabicyclo[2.2.2]octane) as anti-fading agent. Sections were viewed using a Zeiss Axioimager M2 with a 63x/1.40 oil immersion objective. Images were taken with a sCMOS Orca-flash4.0 camera (Hamamatsu). Contrast and brightness were adapted using Photoshop software.

For simultaneous double labeling with fluorescence and gold markers, sections mounted on slot grids were incubated with mouse anti-xyloglucan antibodies (1:10) as described above. Thereafter, sections were labeled with goat anti-mouse IgG coupled to 6 nm gold (6 min), directly followed by incubation with goat anti-mouse IgG coupled to Cy3. There were enough unbound first antibodies left for fluorochrome coupled marker molecules. Slot grids were then stained with DAPI and mounted on a slide under a coverslip with two additional coverslips laterally placed as spacer (in 50% glycerol) and fluorescent images were taken (see above). Thereafter, sections were washed with double distilled water and stained with 1% aqueous uranyl acetate (5 min) and in some cases with lead citrate (15-30 sec). Stained sections were examined in a Jeol TEM (see below). Alignment and overlay of light microscopic and electron microscopic images were performed with Picture Overlay Program (Jeol). Background was negligible in control experiments without first antibody. Contrast and brightness were adapted using Photoshop software.

Phylogenetic Tree Generation

Sequences of the plasma membrane-type Qa-SNAREs were acquired from NCBI (https://ncbi.nlm.nih.gov/BLAST) or from Phytozome v12 (https://phytozome.jgi.doe.gov/pz/portal.html) using taxa with complete genome sequences representative of the major plant branches. Proteins were aligned using MUSCLE in MEGA7 (Kumar et al., 2016). Phylogeny was tested using Neighbor-Joining (NJ) method (Seitou and Nei, 1987) in MEGA7. The optimal tree for just plant sequences had a branch length sum of 32.49052963, while the tree with additional non-plant taxa was 35.15907422. The percentage of replicate trees in which the associated taxa clustered together in the bootstrap test (100 replicates) is shown next to the branches (Felsenstein, 1985). The tree is drawn to scale, with branch lengths in the same units as those of the evolutionary distances used to infer the phylogenetic tree. The evolutionary distances were computed using the Poisson correction method (Zuckerkandl and Pauling, 1965) and are in the units of the number of amino acid substitutions per site. The rate variation among sites was modeled with a gamma distribution (shape parameter = 1). The analysis involved 106 amino acid sequences. All ambiguous positions were removed for each sequence pair. There were a total of 541 positions in the final dataset.

Phenotypic Analysis

Seedlings and whole-mount chloral hydrate preparations of embryos were analyzed using a Leica MZFLIII binocular or a ZEISS Axiophot microscope (Heese et al., 2001). For structural analysis of endosperms, ovules were fixed in 4% paraformaldehyde, dehydrated with a series of ethanol and embedded in LR-White Resin (Figures 6I–6K) or Epon (Figure 6L). 1 to 5 μm-cut slices using cryomicrotome (Supercut 2065) were stained with toluidine blue. Images were taken with a Leica DC200 camera, using Adobe Photoshop CS3, or an AxioCam, using AxioVision 4.8.1 software. Images were processed with Adobe Photoshop CS3 and CS5.

Developmental Cell, Volume *44*

Supplemental Information

Concerted Action of Evolutionarily Ancient and Novel SNARE Complexes in Flowering-Plant Cytokinesis

Misoon Park, Cornelia Krause, Matthias Karnahl, Ilka Reichardt, Farid El Kasmi, Ulrike Mayer, York-Dieter Stierhof, Ulrike Hiller, Georg Strompen, Martin Bayer, Marika Kientz, Masa H. Sato, Marc T. Nishimura, Jeffery L. Dangl, Anton A. Sanderfoot, and Gerd Jürgens

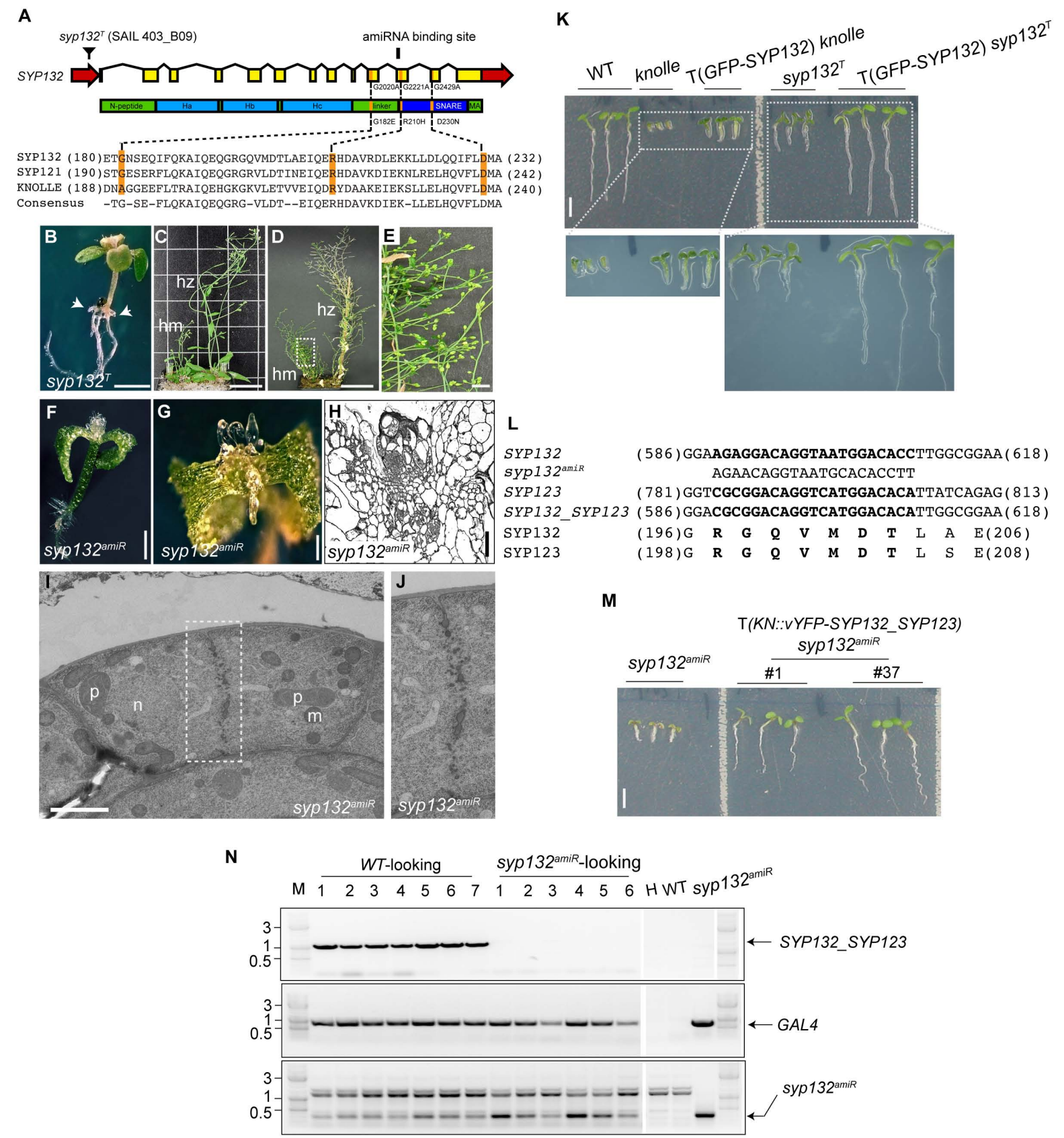
A
syp132T (SAIL 403_B09)
amiRNA binding site
SYP132
G2020A G2221A G2429A
N-peptide Ha Hb Hc linker SNARE MA
G182E R210H D230N
SYP132 (180)ETGNSEQIFQKAIQEQGRGQVMDTLAEIQERHDAVRDLEKKLLDLQQIFLDMA (232)
SYP121 (190)STGESERFLQKAIQEQGRGRVLDTINEIQERHDAVKDIEKNLRELHQVFLDMA (242)
KNOLLE (188)DNAGGEEFLTRAIQEHGKGKVLETVVEIQDRYDAAKEIEKSLLELHQVFLDMA (240)
Consensus -TG-SE-FLQKAIQEQGRG-VLDT--EIQERHDAVKDIEK-LLELHQVFLDMA
B
syp132T
C
hz
hm
D
hz
hm
E
F
syp132amiR
G
syp132amiR
H
syp132amiR
I
p
n
p
m
syp132amiR
J
syp132amiR
K
WT
knolle
T(GFP-SYP132) knolle
syp132T
T(GFP-SYP132) syp132T
L
SYP132 (586)GGAAGAGGACAGGTAATGGACACCTTGGCGGAA(618)
syp132amiR AGAACAGGTAATGCACACCTT
SYP123 (781)GGTCGCGGACAGGTCATGGACACATTATCAGAG(813)
SYP132_SYP123 (586)GGACGCGGACAGGTCATGGACACATTGGCGGAA(618)
SYP132 (196)G R G Q V M D T L A E(206)
SYP123 (198)G R G Q V M D T L S E(208)
M
T(KN::vYFP-SYP132_SYP123)
syp132amiR
syp132amiR
#1
#37
N
WT-looking
syp132amiR-looking
M 1 2 3 4 5 6 7 1 2 3 4 5 6 H WT syp132amiR
3
1
0.5
SYP132_SYP123
GAL4
syp132amiR

Figure S1, Related to Figure 1. Different attempts to generate mutations in the *SYP132* gene

(A) Schematic view of the *SYP132* gene organization and the site of the T-DNA insertion (SAIL 403_B09). The position of the amiRNA is also indicated as well as the TILLING variants. Yellow boxes, exons; red arrows, 5' UTR and 3' UTR. (**B-E**) *syp132*^{T} mutant phenotypes: (**B**) seedling; arrowheads, lateral roots; (**C-E**) adult plants; note bushy appearance of *syp132*^{T} homozygous (hm) plants compared to heterozygous (hz) plants (**C, D**) and flowers with compromised fertility (**E**). (**F-J**) *syp132*^{amiR} mutant phenotypes*:* (**F-G**) seedlings; (**H**) section through shoot end of seedling; (**I-J)** TEM images after cryo-fixation and freeze-substitution of mutant embryos; (**J**) magnified area boxed in (**I**). n, nucleus; m, mitochondrion; p, proplastid. (**K**-**N**) Complementation tests. (**K**) *SYP132::GFP-SYP132* transgene (T) in *syp132*^{T} *or knolle* mutant seedlings (see Table S3 for genetic analysis). The lower panels show boxed areas (*upper panels*) at higher magnification. Note that *SYP132::GFP-SYP132* partially rescues *knolle* mutant and fully complements *syp132*^{T} mutant. (**L**-**N**) Complementation test of *KNOLLE::vYFP(vY)-SYP132_SYP123* transgene (T) in *syp132*^{amiR} *mutant*. (**L**) The relevant nucleotide sequences of *SYP132, syp132*^{amiR}*, SYP123* and a chimeric construct (*SYP132_SYP123*) are shown. The corresponding peptide sequences of *SYP132 and SYP123* are also shown for comparison. Note that the peptide sequence of SYP132_SYP123 is the same as that of SYP132, although the nucleotide sequences are different. (**M**) Seedlings of two independently rescued lines. *syp132*^{amiR} is shown as control (*left*). (**N**) Genotyping analysis of rescued seedlings. Genomic DNA was isolated individually from seven wild type (WT)-looking and six *syp132*^{amiR}-looking seedlings among F1 progenies and subjected to PCR. Note that wild type-looking seedlings bear the chimeric transgene in the *syp132*^{amiR} mutant background. H, no template; WT, wild-type; M, molecular marker (kilobases). Scale bars, 5 mm (**B**, **E**); 3 cm (**C**, **D**); 1 mm (**F**); 500 µm (**G**); 50 µm (**H**); 2 µm (**I**); 5 mm (**K**, **M**).

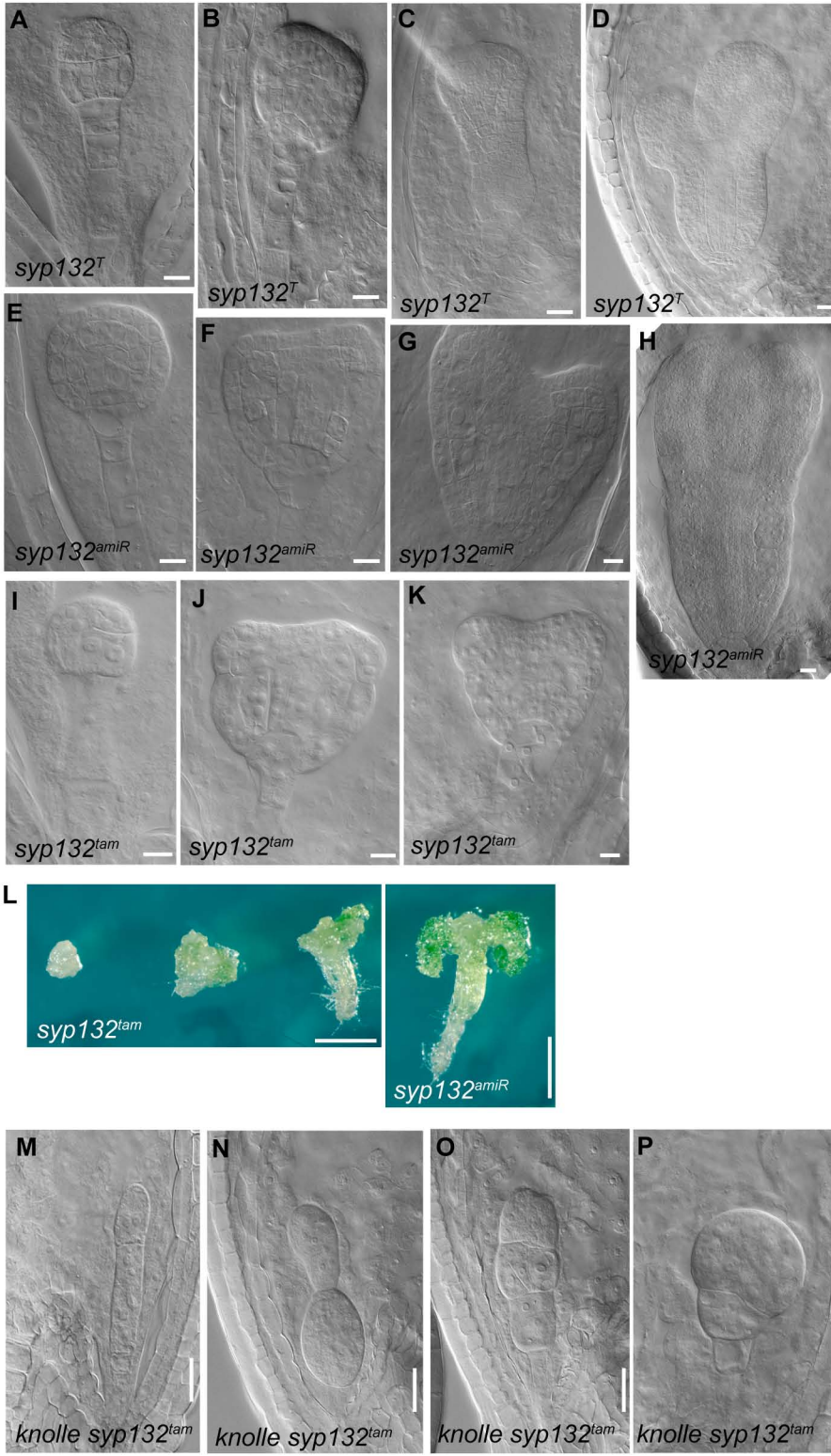
A
syp132T
B
syp132T
C
syp132T
D
syp132T
E
syp132amiR
F
syp132amiR
G
syp132amiR
H
syp132amiR
I
syp132tam
J
syp132tam
K
syp132tam
L
syp132tam
syp132amiR
M
knolle syp132tam
N
knolle syp132tam
O
knolle syp132tam
P
knolle syp132tam

Figure S2, Related to Figure 1. Detailed images of *syp132* single and *knolle syp132* double mutants

(**A**-**K**) Embryos of *syp132* single mutants: (**A**-**D**) *syp132*^{T} at different stages; (**E**-**H**) *syp132*^{amiR} at different stages; (**I**-**K**) *syp132*^{tam}. (**L**) Seedling phenotypes of *syp132*^{tam}. Note the *syp132*^{tam} mutant presents variable, stronger defects than the single *syp132*^{amiR} mutant (**L**, *right*). (**M**-**P**) Embryos of *knolle syp132*^{tam} double mutants. Scale bars, 10 μm (**A**-**K**, **M**-**P**); 1 mm (**L**).

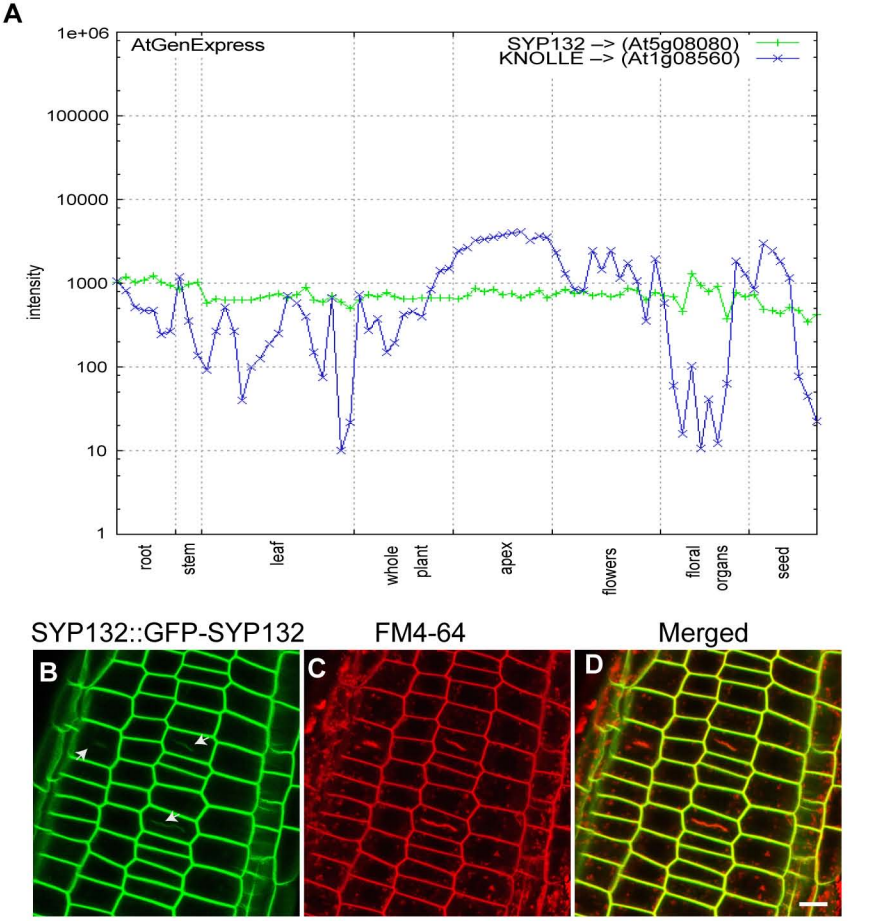

Figure S3, Related to Figure 3. Expression and localization of SYP132

(**A**) Expression profiles of the Qa-SNAREs *SYP132* (At5g08080, green) and *KNOLLE* (At1g08560, blue); data from AtGenExpress (http://jsp.weigelworld.org/expviz/expviz.jsp) (Schmid et al., 2005). Note ubiquitous expression of *SYP132* in contrast to *KNOLLE*, which is only present in dividing tissues. (**B**-**D**) Live imaging of GFP-tagged SYP132 (**B**, green), expressed from its own promoter, in seedling roots counterstained with the endocytic tracer FM4-64 (**C**, red); (**D**) SYP132 co-localizes with FM4-64 at the plasma membrane and weakly labels the cell plate (arrows) in dividing cells. Scale bar, 5 µm in (**D**).

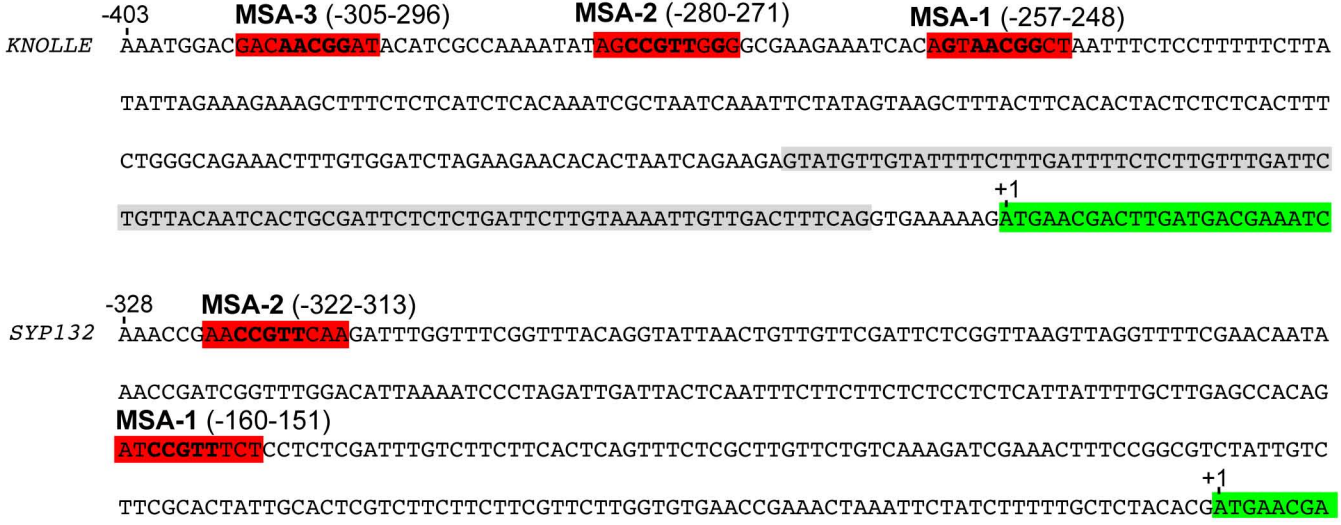

Figure S4, Related to Figure 3. MSA sequences in the *KNOLLE* and *SYP132* promoters
Mitosis-specific activator (MSA) sequences in the promoter regions of *KNOLLE* and *SYP132*. Red box, MSA sequence, the conserved sequence in the MSA (a/g a/g CCGTT a/g G a/g) is in bold letters; grey box, intron; green box, start of coding sequence. Numbers indicate the position of nucleotides in relation to the translational start (+1). Note that the MSA-3 and MSA-1 elements in *KNOLLE* are reverse oriented.

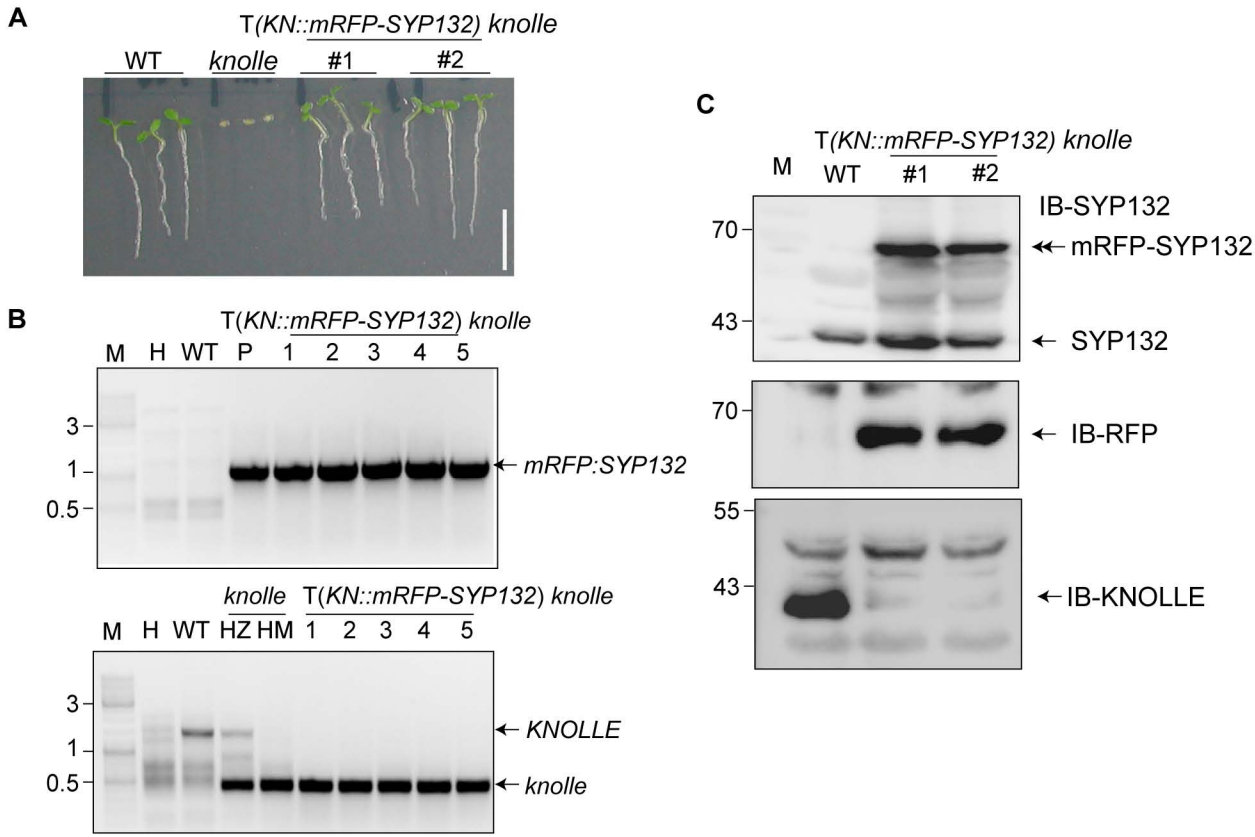

Figure S5, Related to Figure 6. Complementation of knolle knockout mutant by *KNOLLE::mRFP-SYP132* transgene

(**A**) Seedlings from two independent *knolle* mutant rescue lines bearing the *KNOLLE(KN)::mRFP-SYP132* transgene (T). Note that the rescued seedlings are phenotypically indistinguishable from *Col* wild type (WT). *knolle* mutant seedlings are shown as control. Scale bar, 5 mm. (**B**) Genotyping analysis of rescued seedlings. Genomic DNA was isolated individually from five offspring plants and subjected to PCR for the transgene (*upper panel*) and for *KNOLLE* wild-type and *knolle* mutant alleles (*lower panel*). H, no template; WT, wild-type; P, *KNOLLE::mRFP-SYP132* plasmid, HZ, *knolle* heterozygotes; HM, *knolle* homozygotes; M, molecular markers (kilobases). (**C**) Immunoblot analysis. Total protein lysates of seedlings from two independent *knolle* mutant rescue lines bearing the *KNOLLE(KN)::mRFP-SYP132* transgene (T) were subjected to immunoblot (IB) analysis using anti-SYP132, anti-RFP and anti-KNOLLE antisera. *Upper panel*: mRFP-SYP132 (double-headed arrow) and endogenous SYP132 (single arrow) were detected in the same anti-SYP132 immunoblot. Non-transformed wild type (WT) seedlings are shown as control. M, molecular markers (kilodaltons indicated on the left).

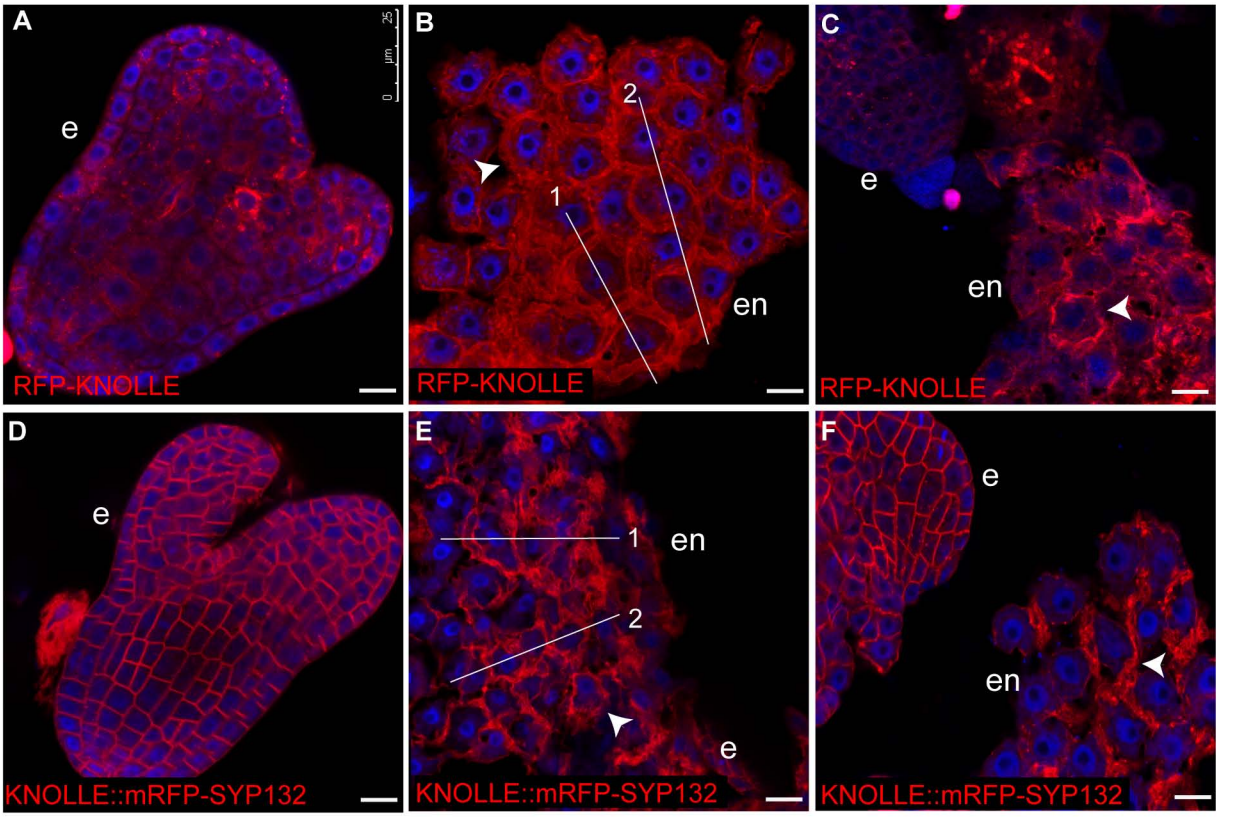

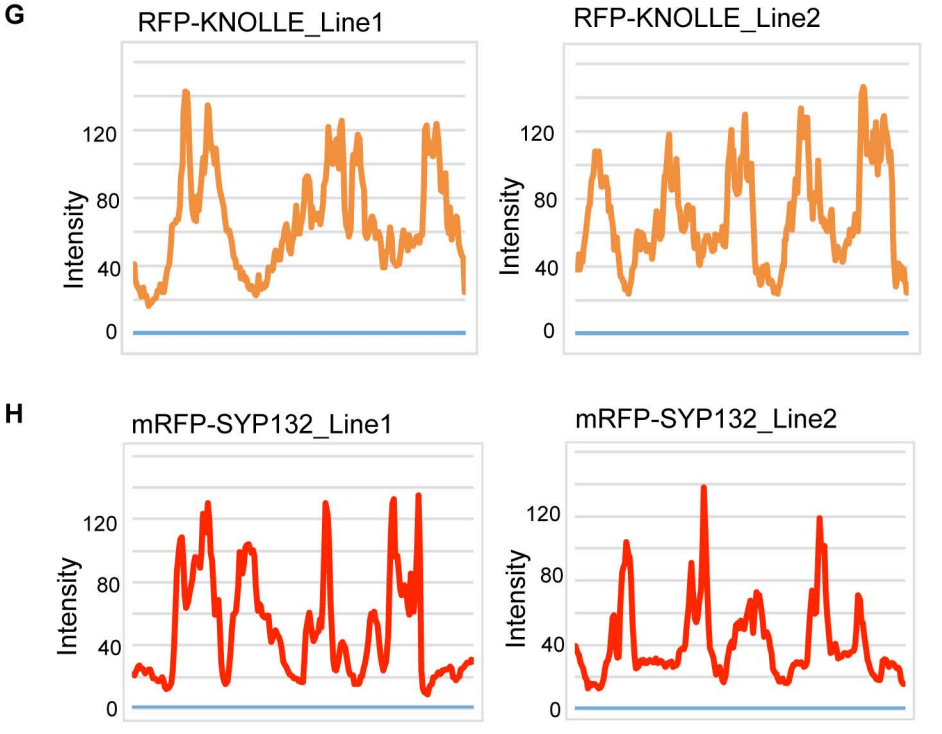

Figure S6, Related to Figure 6. Expression of SYP132 and KNOLLE proteins in cellularizing endosperm

Subcellular localization of KNOLLE::RFP-KNOLLE (**A**-**C**) and KNOLLE::mRFP-SYP132 *knolle* (**D**-**F**) in ovules containing developing embryos and cellularizing endosperm. Whole-mount preparations were labelled by immunofluorescence with anti-RFP antibody (red). Nuclei were counterstained with DAPI (blue). e, embryo; en, endosperm. Arrowheads indicate partioning membranes in cellularizing endosperm (**B**, **C**, **E**, **F**). Scale bars, 10 µm (**A**-**F**). (**G**, **H**) Quantification analysis of signal intensity profiles across cellularizing endosperm (along lines 1 and 2 in **B**, **E**).

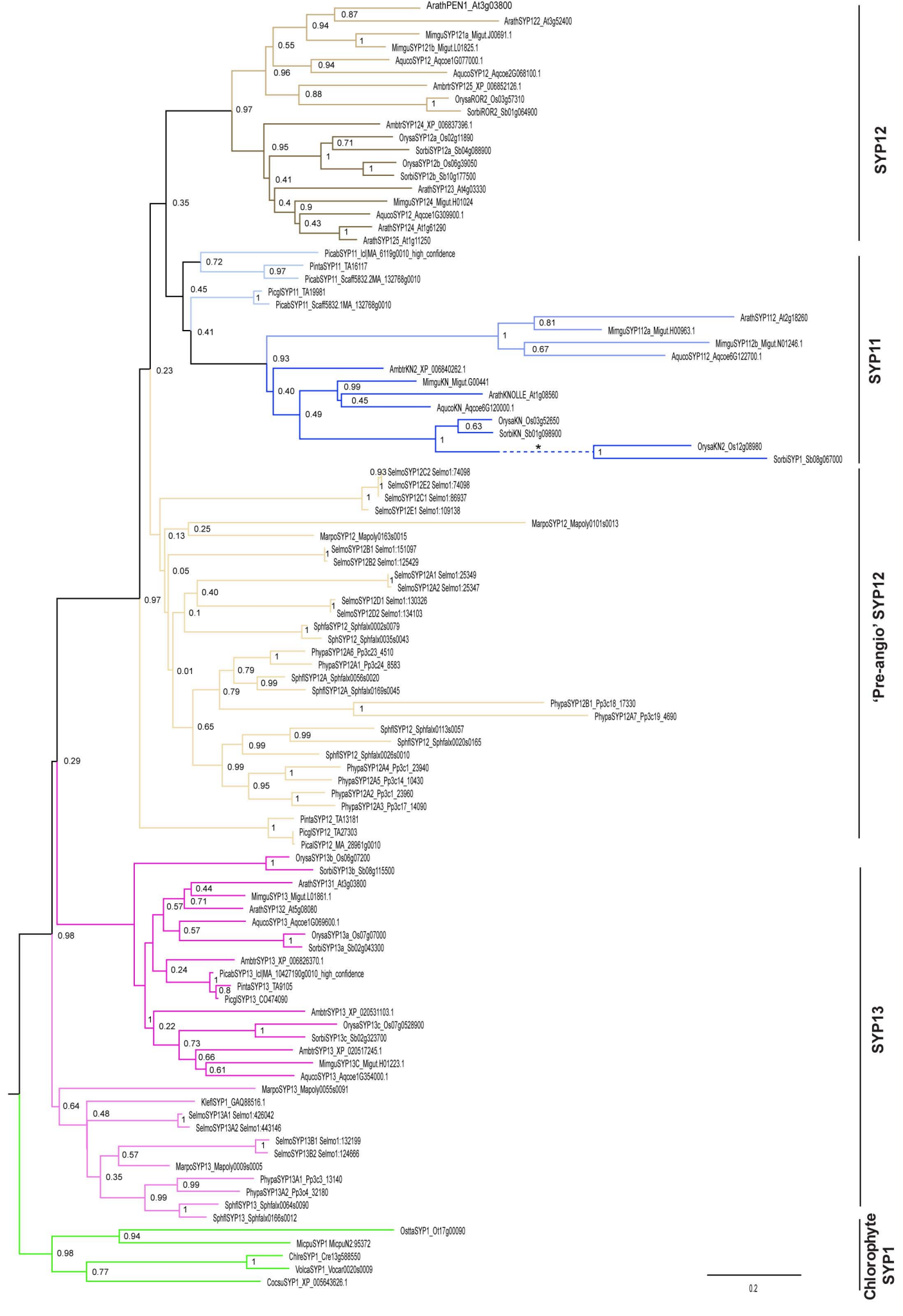
ArathPEN1_At3g03800
ArathSYP122_At3g52400
MimguSYP121a_Migut.J00691.1
MimguSYP121b_Migut.L01825.1
AqucoSYP12_Aqcoe1G077000.1
AqucoSYP12_Aqcoe2G068100.1
AmbtrSYP125_XP_006852126.1
OrysaROR2_Os03g57310
SorbiROR2_Sb01g064900
AmbtrSYP124_XP_006837396.1
OrysaSYP12a_Os02g11890
SorbiSYP12a_Sb04g088900
OrysaSYP12b_Os06g39050
SorbiSYP12b_Sb10g177500
ArathSYP123_At4g03330
MimguSYP124_Migut.H01024
AqucoSYP12_Aqcoe1G309900.1
ArathSYP124_At1g61290
ArathSYP125_At1g11250
PicabSYP11_lcl|MA_6119g0010_high_confidence
PintaSYP11_TA16117
PicabSYP11_Scaff5832.2MA_132768g0010
PicglSYP11_TA19981
PicabSYP11_Scaff5832.1MA_132768g0010
ArathSYP112_At2g18260
MimguSYP112a_Migut.H00963.1
MimguSYP112b_Migut.N01246.1
AqucoSYP112_Aqcoe6G122700.1
AmbtrKN2_XP_006840262.1
MimguKN_Migut.G00441
ArathKNOLLE_At1g08560
AqucoKN_Aqcoe6G120000.1
OrysaKN_Os03g52650
SorbiKN_Sb01g098900
OrysaKN2_Os12g08980
SorbiSYP1_Sb08g067000
SelmoSYP12C2 Selmo1:74098
SelmoSYP12E2 Selmo1:74098
SelmoSYP12C1 Selmo1:86937
SelmoSYP12E1 Selmo1:109138
MarpoSYP12_Mapoly0101s0013
MarpoSYP12_Mapoly0163s0015
SelmoSYP12B1 Selmo1:151097
SelmoSYP12B2 Selmo1:125429
SelmoSYP12A1 Selmo1:25349
SelmoSYP12A2 Selmo1:25347
SelmoSYP12D1 Selmo1:130326
SelmoSYP12D2 Selmo1:134103
SphfaSYP12_Sphfalx0002s0079
SphSYP12_Sphfalx0035s0043
PhypaSYP12A6_Pp3c23_4510
PhypaSYP12A1_Pp3c24_8583
SphflSYP12A_Sphfalx0056s0020
SphflSYP12A_Sphfalx0169s0045
PhypaSYP12B1_Pp3c18_17330
PhypaSYP12A7_Pp3c19_4690
SphflSYP12_Sphfalx0113s0057
SphflSYP12_Sphfalx0020s0165
SphflSYP12_Sphfalx0026s0010
PhypaSYP12A4_Pp3c1_23940
PhypaSYP12A5_Pp3c14_10430
PhypaSYP12A2_Pp3c1_23960
PhypaSYP12A3_Pp3c17_14090
PintaSYP12_TA13181
PicglSYP12_TA27303
PicalSYP12_MA_28961g0010
OrysaSYP13b_Os06g07200
SorbiSYP13b_Sb08g115500
ArathSYP131_At3g03800
MimguSYP13_Migut.L01861.1
ArathSYP132_At5g08080
AqucoSYP13_Aqcoe1G069600.1
OrysaSYP13a_Os07g07000
SorbiSYP13a_Sb02g043300
AmbtrSYP13_XP_006826370.1
PicabSYP13_lcl|MA_104271g0010_high_confidence
PintaSYP13_TA9105
PicglSYP13_CO474090
AmbtrSYP13_XP_020531103.1
OrysaSYP13c_Os07g0528900
SorbiSYP13c_Sb02g323700
AmbtrSYP13_XP_020517245.1
MimguSYP13C_Migut.H01223.1
AqucoSYP13_Aqcoe1G354000.1
MarpoSYP13_Mapoly0055s0091
KlefiSYP1_GAQ88516.1
SelmoSYP13A1 Selmo1:426042
SelmoSYP13A2 Selmo1:443146
SelmoSYP13B1 Selmo1:132199
SelmoSYP13B2 Selmo1:124666
MarpoSYP13_Mapoly0009s0005
PhypaSYP13A1_Pp3c3_13140
PhypaSYP13A2_Pp3c4_32180
SphflSYP13_Sphfalx0064s0090
SphflSYP13_Sphfalx0166s0012
OsttaSYP1_Ot17g00090
MicpuSYP1 MicpuN2:95372
ChreSYP1_Cre13g588550
VolcaSYP1_Vocar0020s0009
CocsuSYP1_XP_005643626.1
SYP12
SYP11
'Pre-angio' SYP12
SYP13
Chlorophyte SYP1
0.2

Figure S7, Related to Figure 7. Extended phylogenetic tree of plant SYP1 Qa-SNAREs

Proteins were aligned using MUSCLE in MEGA7. Phylogeny was tested using the Neighbor-Joining method in MEGA7. Arath, *Arabidopsis thaliana* (eudicot:rosid); Mimgu, *Mimulus guttatus* (eudicot:asterid); Aquco, *Aquilegia coerulea* (basal eudicot); Orysa*, Oryza sativa*, Sorbi, *Sorghum bicolor* (monocots); Ambtr, *Amborella trichopoda* (basal angiosperm); Picab, *Picea abies* (gynmosperm); Pinta, *Pinus taeda*; Picgl, *Picea glauca*; Selmo, *Selaginella moellendorffii* (lycopod); Sphfl, *Sphagnum flexuosum* (moss)*;* Phypa, *Physcomitrella patens* (moss); Marpo, *Marchantia polymorpha* (liverwort); *Klebsormidium flaccidum* (charophyte algae); Chlre, *Chlamydomonas reinhardtii*, Volca, *Volvox carteri*; Cocsu, *Coccomyxa subellipsoidea*; Ostta, *Ostreococcus tauri;* Micpu, *Micromonas pusilla* (chlorophyte algae). Names of the SYP1 clades are after Sanderfoot (2007). Note the scale of the *Oryza* SYP11 branch was shortened to 33% (asterisk).

Supplementary Tables

Table S1, Related to Figures 1, 4 and 5. Quantitative analysis of SNARE double mutants: embryo phenotypes*

Genotypes segregating in F1	wild-type [a]	*knolle*	double mutant [b]	N
kn	75% (193)	25% (63)		256
kn syp132^{amiR}	77% (545)	18% (129)	5% (35)	709
kn syp132^{T} ***	75% (498)	18% (118)	7% (48)	664
kn syp132^{tam}	68% (1489)	17% (367)	15% (341)	2197
kn npsn11	75% (381)	19% (97)	6% (32)	510
kn snap33	74% (351)	18% (86)	8% (40)	477
kn syp71^{amiR}	76% (356)	17% (79)	7% (34)	469

[a] Embryos of homozygous single mutants of *syp132^{amiR}*, *syp132^{T}*, *npsn11*, *snap33* and *syp71^{amiR}* display no obvious or very mild abnormalities and were phenotypically classified as wild-type.
[b] Homozygous double mutant embryos show an enhanced *knolle (kn)* phenotype, consisting of only a few multi-nucleate cells (for images, see Figures 1, 4 and 5 and Figure S2). The expected value for homozygous double mutants is 6.25%.
*** *syp132^{T}* heterozygous plants produced 24% homozygous mutant progeny (N=390). These adult plants were smaller than wild-type, bushy and hardly made any seeds (see Fig. S1B-E).

*** Note:** The embryos analyzed were F1 progenies of the following plant genotypes:

Genotypes segregating in F1	Parental genotypes
kn	*kn/KN* (self-pollinated)
syp132^{amiR}	*RPS5A::GAL4/- × UAS::amiRNA(SYP132)/-*
syp132^{T}	*syp132^{T}/-* (self-pollinated)
kn syp132^{amiR}	*kn/KN RPS5A::GAL4/- × kn/KN UAS::amiRNA(SYP132)/-*
kn syp132^{T}	*kn/KN syp132^{T}/SYP132* (self-pollinated)
kn syp132^{tam}	*kn/KN RPS5A::GAL4/- syp132^{T}/-*
kn npsn11	*kn/KN npsn11/NPSN11* (self-pollinated)
kn snap33	*kn/KN snap33/SNAP33* (self-pollinated)
kn syp71^{amiR}	*kn/KN RPS5A::GAL4/- × kn/KN UAS::amiRNA(SYP71)/-*

Whole-mount preparations of heart-stage embryos were phenotypically classified as either *knolle*, double mutant (i.e. enhanced *knolle*) or wild-type by light microscopy.

Table S2, Related to Figures 1, 4 and 5. Quantitative analysis of SNARE double mutants: seedling phenotypes*

genotypes segregating in F1	wild-type	*syp132^{amiR}*	*syp132^{T}*	*knolle*	*snap33*	*syp71^{amiR}*	aborted seeds [a]	N
syp132^{amiR}	74% (642)	25% (216)					1% (11)	869
syp132^{T} *	76% (297)		24% (94)					390
kn	75% (208)			23% (63)			2% (6)	277
kn npsn11	73% (251) [b]			18% (62)			9% (31)	344
kn snap33	57% (229) [c]			17% (70)	18% (74)		8% (32)	405
kn syp71^{amiR}	55% (266) [c]			17% (81)		17% (82)	11% (53)	482

[a] In aborted seeds, embryo development stops and thus they do not germinate. This category includes all homozygous double mutants (expected value 6.25%) and occasionally also a few homozygous single mutants or wild-type.
[b] Phenotypic classification as wild-type also includes homozygous *npsn11* single mutant seedlings which are morphologically indistinguishable from wild-type.
[c] Homozygous single mutant seedlings of *snap33* (necrotic lesions; Heese et al., 2001) and *syp71^{amiR}* (dwarfish; El Kasmi et al., 2013) are abnormal and therefore grouped into separate phenotypic classes, respectively. Expected values are 56.25% for wild-type, 18.75% for each genotype of homozygous single mutants and 6.25% for homozygous double mutants.
* *syp132^{T}* heterozygous plants produced 24% homozygous mutant progeny (N=390). These adult plants were smaller than wild-type, bushy and hardly made any seeds (see Fig. S1B-E).

*** Note**: The seedlings analyzed were F1 progenies of the following plant genotypes:

Genotypes segregating in F1	Parental genotypes
kn	*kn/KN* (self-pollinated)
syp132^{amiR}	*RPS5A::GAL4/-* × *UAS::amiRNA(SYP132)/-*
syp132^{T}	*syp132^{T}/-* (self-pollinated)
kn syp132^{amiR}	*kn/KN RPS5A::GAL4/-* × *kn/KN UAS::amiRNA(SYP132)/-*
kn syp132^{T}	*kn/KN syp132^{T}/-* (self-pollinated)
kn npsn11	*kn/KN npsn11/NPSN11* (self-pollinated)
kn snap33	*kn/KN snap33/SNAP33* (self-pollinated)
kn syp71^{amiR}	*kn/KN RPS5A::GAL4/-* × *kn/KN UAS::amiRNA(SYP71)/-*

Phenotypic classification of seedling progenies was validated by genotyping (at least five) individual seedlings or plants representative for each class.

Table S3, Related to Figure 6 and Figures S1 and S5. Complementation tests of *SYP132::GFP-SYP132 and KN::mRFP-SYP132*

T1 plants		T2 plants				
Transgenes	Allele	*WT*	*knolle*	*syp132^{T}*	Partial-Rescued	N
SYP132::GFP-SYP132 #1	*kn*/+	85%(260)	3% (10)		12% (37)	307
SYP132::GFP-SYP132 #2	*kn*/+	87% (350)	2% (9)		11% (42)	401
SYP132::GFP-SYP132 #1	*syp132^{T}*/-	94% (303)		6% (19)		322
SYP132::GFP-SYP132 #2	*syp132^{T}*/-	95% (353)		5% (18)		371
KN::mRFP-SYP132 #1	*kn*/+	96% (374)	4% (16)*			390
KN::mRFP-SYP132 #2	*kn*/+	95% (495)	5% (26)*			521

*The segregation ratio of *knolle (kn)* mutant will be ideally 6.25% if a transgene fully rescues the mutant. Note that the actual number is slightly less than the expected number.

Table S4, Oligonucleotides, Related to STAR Methods

Primer name	Sequence 5' – 3'	remark
NPSN11 LP	GTCTTATTAGCTTCAAGTAAGTCTT	genotyping (*npsn11*)
NPSN11 RP	CTGAGCCTTGAGAGCTGCTGAAGTATC	genotyping (*npsn11*)
LBa1	TGGTTCACGTAGTGGGCCATC	genotyping (*npsn11*)
TAG3	CTGATACCAGACGTTGCCCGCATAA	genotyping (*snap33*)
MH48 – SP2	GAACCGACTGGTTTTCAATACCACC	genotyping (*snap33*)
GM S25 – FW4	GCTAGATCCTGGGCTTTCGATTTG	genotyping (*snap33*)
X37-2 CIII	AAGGCTCTCTGGGACTCCGG	genotyping (*knolle*)
X37-2 DIII	GGGATGGATATGGTGGTGC	genotyping (*knolle*)
GAL4s	GAAGCTCCTGTCCTCCATCGA	genotyping (*GAL4*)
GAL4as	CTTTGTTCACGTTGTCCTGGA	genotyping (*GAL4*)
SAIL 403_B09 F	TGATATTCCGAAATCGACTGC	genotyping (*syp132*^{T})
SAIL 403_B09 R	TTGAACCTAGCAAGACAAAGAGG	genotyping (*syp132*^{T})
SAIL LB1	GCCTTTTCAGAAATGGATAAATAGCCTTGCTTCC	genotyping (*syp132*^{T})
UASs	TACTGTCCTCCGAGCGGAGTA	genotyping (*syp132*^{amiR})
eGFP-200-reverse	GTGGTGCAGATGAACTTC	genotyping (*syp132*^{amiR})
vYFP700s	ACAACCACTACCTGAGCTACC	genotyping
mRFP700s	CAAGACCGACATCAAGCTGGA	genotyping
amiRNA-A	CTGCAAGGCGATTAAGTTGGGTAAC	cloning (*syp132*^{amiR})
amiRNA-B	GCGGATAACAATTTCACACAGGAAACAG	cloning (*syp132*^{amiR})
amiRNA132 I	GATAGGTGTCCATTACCTGTGCTTCTCTCTTTTGTATTCC	cloning (*syp132*^{amiR})
amiRNA132 II	GAAGCACAGGTAATGGACACCTATCAAAGAGAATCAATG	cloning (*syp132*^{amiR})
amiRNA132 III	GAAGAACAGGTAATGCACACCTTTCACAGGTCGTGATAT	cloning (*syp132*^{amiR})
amiRNA132 IV	GAAAGGTGTGCATTACCTGTTCTTCTACATATATATTCCT	cloning (*syp132*^{amiR})
132 start SmaI	AAA CCC GGG ATG AAC GAT CTT CTG AAG GGT TC	Cloning of *SYP132_SYP123*
Intra-first-antisense	GTCCATGACCTGTCCGCGTCCTTGCTCCTGAATCGC	Cloning of *SYP132_SYP123*
Intra-first-sense	GCGATTCAGGAGCAAGGACGCGGACAGGTCATGGAC	Cloning of *SYP132_SYP123*
Intra-second-	ACGTTCTTGGATTTCCGCTAATGTGTCCATGACCTG	Cloning of *SYP132_SYP123*
Intra-second-sense	CAGGTCATGGACACATTAGCGGAAATCCAAGAACGT	Cloning of *SYP132_SYP123*
132 stop EcoR1	AAA GAA TTC TCA AGC ACT CTT GTT TTT CCA A	Cloning of *SYP132_SYP123*
132 Tilling F	GGCGAGTTTATACAGGTA	TILLING (primer pair 1)
132 Tilling R	CCTCAAGCACTCTTGTTT	TILLING (primer pair 1)
132 Tilling F2	ACCGTAACAATAGTACCG	TILLING (primer pair 2)
132 Tilling R2	GCAACCACAATGAGGAGG	TILLING (primer pair 2)
KNOLLE-R218H	CATCATAATGGTCTTGAATCTCAACCACAGTTTC	site directed mutagenesis
KNOLLE-D238N	CAGCCATATTAAGAAACACTTGGTGAAGC	site directed mutagenesis

Sequence name	**Sequence 5' – 3'**	
SYP132 original sequence	AGGACAGGTAATGGACACCTT	
amiRNAas	AGCACAGGTAATGGACACCT	
amiRNA*	AGAACAGGTAATGCACACCTT	